

1 **Repairing a deleterious domestication variant in a floral regulator of tomato by**
2 **base editing**

3

4 Anna N. Glaus^{1,2}, Marion Brechet^{1,2}, Ludivine Lebeigle², Justyna Iwaszkiewicz³, Giovanna
5 Ambrosini^{4,5}, Irene Julca⁶, Jing Zhang⁷, Robyn Roberts⁷, Christian Iseli^{4,5}, Nicolas Guex^{4,5}, José
6 Jiménez-Gómez⁸, Natasha Glover⁶, Gregory B. Martin^{7,9}, Susan Strickler^{7,10,11}, and Sebastian
7 Soyk^{1,2} *

8

9 ¹Department of Plant Molecular Biology, University of Lausanne, 1015 Lausanne, Switzerland

10 ²Center for Integrative Genomics, University of Lausanne, 1015 Lausanne, Switzerland

11 ³Molecular Modeling Group, Swiss Institute of Bioinformatics, 1015 Lausanne, Switzerland

12 ⁴Bioinformatics Competence Centre, University of Lausanne, 1015 Lausanne, Switzerland

13 ⁵Bioinformatics Competence Centre, École Polytechnique Fédérale de Lausanne, 1015 Lausanne,
14 Switzerland

15 ⁶SIB Swiss Institute of Bioinformatics, 1015 Lausanne, Switzerland

16 ⁷Boyce Thompson Institute for Plant Research, Ithaca, NY 14853, USA

17 ⁸Centro de Biotecnología y Genómica de Plantas (CBGP), Madrid, Spain

18 ⁹Plant Pathology and Plant-Microbe Biology Section, School of Integrative Plant Science, Cornell
19 University, Ithaca, NY 14853, USA

20 ¹⁰Plant Science and Conservation Chicago Botanic Garden, Glencoe, IL 60022, USA.

21 ¹¹Plant Biology and Conservation Program Northwestern University, Evanston, IL 60208, USA.

22

23 *Correspondence: sebastian.soyk@unil.ch

24

25 **ABSTRACT**

26 Crop genomes accumulated deleterious mutations, a symptom known as the cost of domestication.
27 Precision genome editing has been proposed to eliminate such potentially harmful mutations,
28 however, experimental demonstration is lacking. Here, we identified a deleterious mutation in the
29 tomato transcription factor *SUPPRESSOR OF SP2* (*SSP2*), which became prevalent in the
30 domesticated germplasm and diminished DNA-binding to genome-wide targets. We found that
31 *SSP2* acts partially redundant with its paralog *SSP* to regulate shoot and inflorescence architecture.
32 However, redundancy was compromised during tomato domestication and completely lost in the
33 closely-related species *Physalis grisea*, in which a single ortholog regulates shoot branching. We
34 applied base editing to directly repair the deleterious mutation in cultivated tomato and obtained
35 plants with compact growth that provide an early fruit yield. Our work shows how deleterious
36 variants sensitized modern genotypes for phenotypic tuning and illustrates how repairing
37 deleterious mutations with genome editing allows for predictable crop improvement.

38

39 INTRODUCTION

40 Deleterious mutations lead to the alteration or loss of gene activity. Crop domestication has been
41 accompanied by an accumulation of potentially deleterious mutations^{1,2}, a phenomenon described
42 as the genetic cost of domestication³. Such potentially harmful variants likely influence many
43 important agricultural traits⁴. For example, harmful recessive alleles can have detrimental effects
44 that are exposed in homozygous progeny during inbreeding⁵. Deleterious mutations are often
45 considered to mainly negatively affect fitness of natural populations but recently, a more nuanced
46 view has been proposed that considers their adaptive value^{6,7}. Deleterious, loss-of-function
47 mutations may confer an evolutionary advantage during rapid shifts in environmental conditions
48 and the selective pressures thereof⁷. Crop domestication created novel environments under which
49 many traits that were beneficial in the wild likely became neutral or even detrimental. Illustrative
50 examples include loss of photoperiodic flowering and seed shattering. These observations support
51 the “less-is-more” idea, which proposes that selection may favor a less-than-complete repertoire
52 of functional genes⁷. Nonetheless, eliminating deleterious variants from domesticated germplasm
53 has been proposed as a major goal in future crop breeding to avert potential harmful effects^{4,5}.
54 However, correcting genetic variants by recombination during cross-breeding can be complicated
55 by genetic linkage with beneficial alleles or near fixation in domesticated populations. Recent
56 advances in precision genome editing promise to facilitate the repair of deleterious variants⁸.
57 However, to our knowledge, an experimental demonstration of precision genome editing for the
58 repair of deleterious variants in domesticated germplasm has been lacking.

59 A recurrent target of selection during crop domestication and breeding are alterations in flowering
60 time⁹. Changes in flowering time allowed the adaptation of crops to novel environments and
61 growing seasons different from their wild ancestors’ origin. The floral transition also influences
62 plant architecture by balancing vegetative and reproductive growth¹⁰. At the molecular level,
63 flowering occurs when the universal flowering hormone, florigen, reaches a critical level that
64 triggers stem cells in the shoot meristems to switch from vegetative to reproductive growth. In the
65 model crop tomato (*Solanum lycopersicum*), florigen is encoded by *SINGLE FLOWER TRUSS*
66 (*SFT*), a homolog of Arabidopsis *FLOWERING LOCUS T (FT)* and member of the
67 *CENTRORADIALIS, TERMINATING FLOWER1, SELF-PRUNING (CETS)* gene family¹¹. While
68 *SFT* promotes the floral transition, *SELF PRUNING (SP)* acts as antiflorigen and opposes the
69 activity of florigen to repress flowering¹². Evidence from rice and Arabidopsis suggests that

70 florigen protein competes with antflorigen for Group-A basic region/leucine zipper (bZIP)
71 transcription factors to form the Florigen Activation Complex (FAC)¹²⁻¹⁴. In tomato, the bZIP
72 transcription factor SUPPRESSOR OF SP (SSP) is a functional FAC component and *ssp* mutations
73 have been used to fine-tune plant architecture for optimized fruit productivity¹⁵. In other crops,
74 mutations in central florigen pathway components have been also selected to change flowering
75 time and shoot architecture⁹. Yet, how deleterious mutations affected key components of the
76 florigen pathway during crop domestication has not been systematically studied.

77

78 RESULTS

79 **Prediction of deleterious variants in central components of the florigen pathway.** To
80 determine the mutational load in domesticated tomato, we generated a chromosome-scale genome
81 assembly for the closely-related wild tomato species *S. pimpinellifolium* (accession LA1589) (see
82 **Online Methods**). We used this wild tomato genome as a reference to identify nonsynonymous
83 mutations across a collection of 82 genomes along the domestication history of tomato, including
84 27 wild tomato species (*S. pimpinellifolium*), 23 landrace (*S. lyc. var. cerasiforme*), and 32
85 domesticated (*S. lycopersicum*) genomes (**Fig. 1a, Table S1**)^{8,16}. We predicted deleterious variants
86 by amino acid conservation modelling and identified 39,132 (23.1 %) nonsynonymous variants
87 with a putative deleterious effect (SIFT-score < 0.05) (**Fig. S1a, b, Table S2**)¹⁷. This analysis
88 indicated that wild species, landrace, and domesticated tomato genomes contain on average 5,114,
89 7,131, and 8,233 homozygous deleterious variants, respectively (**Fig. S1c**). Next, we focused on
90 core components of the FAC¹⁴ and searched for deleterious variants in *CETS* and Group-A bZIP
91 genes (**Fig. S2**)¹⁸. Among all 12 tomato *CETS* genes, we identified three genes with predicted
92 deleterious variants (**Fig. 1b**). Besides two uncharacterized *TERMINATING FLOWER1* (*TFL1*)-
93 like and *MOTHER OF FT* (*MFT*)-like genes, we found the known flowering repressor *SELF-*
94 *PRUNING 5G* (*SP5G*; Solyc05g053850), which contained a predicted deleterious variant in 45 of
95 the genomes (54.9%) (**Table S3**). We also detected the *sp-classic* breeding mutation (P76L) that
96 was predicted to not be deleterious but tolerated, which supports a hypomorphic nature of the
97 mutation¹⁹. Among all 13 tomato Group-A bZIP genes, we identified four uncharacterized abscisic
98 acid responsive element binding factor (*ABF*)-like genes with predicted deleterious mutations (**Fig.**
99 **1c and Fig. S2**). The most frequent predicted deleterious variant affected the bZIP gene

100 Solyc02g061990 and was detected in 36 genomes (43.9%). We concluded from these analyses that
101 several central florigen pathway components have acquired potentially deleterious mutations
102 during tomato domestication.

103 **A missense mutation in the transcription factor *SSP2* was enriched during domestication.** A
104 phylogenetic analysis comparing group-A bZIP proteins of tomato and Arabidopsis showed that
105 Solyc02g061990 is most closely related to *SSP*, thus we named the gene *SSP2* (**Fig. 2a** and **Fig.**
106 **S2**). *SSP* and *SSP2* form a sister clade to the Arabidopsis proteins FD and FD PARALOG (FDP)
107 ²⁰, with *SSP* and FD being the more ancient genes. In Arabidopsis, FD and FDP are involved in
108 flowering control and phytohormone responses^{21,22}. Expression data from different tomato plant
109 tissues showed that *SSP* and *SSP2* had similar expression patterns, suggesting functional
110 redundancy, most notably in secondary (sympodial) shoot meristems (**Fig. 2b**)^{23,24}. The putative
111 deleterious variant in *SSP2* causes a serine-to-phenylalanine (S169 to F169) exchange at a
112 conserved residue in the DNA-binding domain (**Fig. 2c**). We analyzed the distribution of the
113 ancestral (*SSP2*^{S169}) and domesticated (*SSP2*^{F169}) variants across 768 re-sequenced tomato
114 accessions and found that the domesticated allele was absent from wild tomato species. The
115 putative deleterious variant first arose in tomato landraces (*S. lycopersicum* var. *cerasiforme*), was
116 enriched in domesticated genotypes, and nearly fixed in modern fresh-market and processing types
117 (**Fig. 2d**). To genetically test if the putative deleterious variant has an effect on the floral transition,
118 we introgressed the ancestral *SSP2*^{S169} allele into a processing tomato type (cv. M82). We found
119 that near-isogenic lines (NILs) harboring *SSP2*^{S169} flowered earlier on sympodial shoots and
120 developed shoots that grew more compact compared to the wild-type (WT) controls (**Fig. S3a-f**).
121 In addition, we introduced *SSP2*^{S169} into the hypomorphic *ssp*²¹²⁹ mutant¹⁵ to test whether *SSP2*^{S169}
122 acts redundantly with its paralog *SSP*. We found that *SSP2*^{S169} suppressed late-flowering and
123 indeterminate growth of *ssp*²¹²⁹ mutants (**Fig. S3g, h**), suggesting that the ancestral *SSP2*^{S169} allele
124 can compensate for reduced *SSP* activity.

125 **Domesticated *SSP2*^{F169} is compromised in its function as a transcription factor.** We
126 hypothesized that the loss of the conserved serine residue affects the ability of *SSP2* to bind DNA
127 during the regulation of target genes. We modelled the structure of the ancestral (*SSP2*^{S169}) and
128 domesticated (*SSP2*^{F169}) proteins in a homology-based modelling approach^{25,26}. The model
129 predicted that the conserved serine (S169) most likely forms hydrogen bonds with the phosphate
130 backbone of the DNA target sequence whereas a phenylalanine at this position (F169) might

131 increase the distance between the protein and target DNA due to its larger side-chain and
132 hydrophobicity (**Fig. 2e**). To test whether the amino acid exchange affects the transcription factor
133 function of SSP2, we co-expressed SSP2^{F169}, SSP2^{S169} and SSP with SFT in tobacco leaves to
134 quantify their transactivation activity on the upstream regions of *MACROCALYX* (*MC*;
135 Solyc05g056620), *S. lycopersicum FRUITFULL1* (*SIFUL1*, Solyc06g069430), and *SIFUL2*
136 (Solyc03g114830). These genes are homologous to Arabidopsis *APETALA1* and *FRUITFULL*,
137 which have been shown to be activated by FD during the floral transition¹³. None of the effector
138 constructs activated the *MC* reporter, which may result from a non-direct relationship between *MC*
139 and Arabidopsis *API*. However, the *SIFUL1* and *SIFUL2* reporters were significantly activated by
140 both SSP and ancestral SSP2^{S169} while the level of transactivation by SSP2^{F169} was not significant
141 (**Fig. 2f**). Together, these results suggest that the deleterious variant in *SSP2* disrupts the DNA-
142 binding ability of domesticated SSP2^{F169} and compromises its transcription factor function.

143 To determine how the deleterious SSP2^{F169} variant affects binding at genome-wide targets, we
144 performed DNA affinity purification sequencing (DAP-seq) with SSP, ancestral SSP2^{S169} and
145 domesticated SSP2^{F169} as bait proteins²⁷. We identified 14,091 DAP-seq peaks that were
146 significantly enriched ($\log_2FC \geq 3$, $FDR \leq 0.01$) compared to the input controls (**Fig. 3a and Table**
147 **S4**). The majority (7,388) of peaks were shared between SSP and the ancestral SSP2^{S169} but only
148 1,285 peaks were also bound by domesticated SSP2^{F169}. We analyzed the genome-wide
149 distribution of peaks for all three transcription factors and found more than 50% of peaks within
150 proximal regulatory regions (**Fig. 3b**). *De-novo* motif enrichment analysis identified a G-box motif
151 (CACGTG) with a subtle variation for SSP2^{F169} outside the core-motif (**Fig. 3c**). Next, we analyzed
152 genes with proximal peaks (≤ 3 Kbp upstream and ≤ 2 Kbp downstream) and identified 6,485 and
153 4,229 putative target genes for SSP and SSP^{S169}, of which the majority (3,953 genes) were bound
154 by both proteins (**Fig. 3d and Table S5**). In contrast, domesticated SSP2^{F169} bound only 984 and
155 952 of SSP and SSP^{S169} targets, respectively, and 1,377 genes in total. The low number of SSP2^{F169}
156 targets and shared targets with SSP and SSP2^{S169} suggested that the ability of SSP2^{F169} to bind its
157 genome-wide targets is compromised. To support this finding, we quantified binding intensity at
158 target regions based on normalized read coverage. While SSP and SSP2^{S169} displayed similar
159 binding intensities, SSP2^{F169} binding was strongly reduced (**Fig. 3e, f and Fig. S4c, e**).
160 Furthermore, diminished binding of SSP2^{F169} at SSP2^{S169} and SSP targets was also obvious at the
161 level of individual genes. For example, we found that the upstream regions of the two tomato

162 homologs of *GIGANTEA* (*GI*), which regulates flowering in Arabidopsis²⁸, were bound by SSP
163 and SSP2^{S169} but not by the domesticated SSP2^{F169} variant (**Fig. 3g, h**). Together, our genome-
164 wide binding data demonstrates that SSP and the ancestral SSP2^{S169} variant bind a set of largely
165 shared targets while domesticated SSP2^{F169} is compromised in its ability to bind the targets of the
166 ancestral protein.

167

168 **SSP2 acts partially redundant with SSP to regulate shoot and inflorescence architecture.** To
169 genetically explore the function of *SSP2*, we used CRISPR-Cas9 genome editing and generated
170 *ssp2^{CR}* and *ssp^{CR}* null mutants in two determinate cultivars (**Fig. S5a-b**). The *ssp^{CR}* mutants
171 flowered later than the WT and developed indeterminate shoots, which confirmed previous
172 findings that *SSP* promotes the floral transition (**Fig. 4a-c** and **S5c-e**)¹⁵. We did not observe
173 obvious differences in flowering time for *ssp2^{CR}* single mutants, which supports a diminished
174 activity of SSP2^{F169} in domesticated tomato (**Fig. 4a, c** and **S5c-d**). However, *ssp^{CR}ssp2^{CR}* double
175 mutants tended to flower later than the *ssp^{CR}* single mutant, although at high variability (**Fig. 4c**
176 **and S5c, d**). This phenotypic enhancement became more pronounced on sympodial shoots. Double
177 *ssp^{CR}ssp2^{CR}* mutants produced more leaves on sympodial shoots and more flowers on flowering
178 shoots (inflorescences). We concluded that domesticated SSP2^{F169} is a partial loss-of-function
179 allele and that *SSP* and *SSP2* act partially redundant to promote the transition of meristems to
180 reproductive growth (**Fig. 4d, e**).

181 To obtain molecular insights into how *SSP* and *SSP2* promote meristem transitions, we sequenced
182 mRNA from micro-dissected meristems at the transition (TM) stage of meristem maturation of the
183 *ssp^{CR}* and *ssp2^{CR}* single and double mutants, and the WT (in cv. M82)¹⁵. Clustering of samples in
184 a principal component analysis (PCA) was consistent with the mutant phenotypes that indicated a
185 delayed transition of *ssp^{CR}ssp2^{CR}* double mutants compared to the *ssp^{CR}* single mutant (**Fig. 4f**).
186 We identified 1,832 differentially expressed genes (DEGs) that changed in expression by more
187 than 1.5-fold in at least one of the mutants compared to the WT (FDR ≤ 0.05) (**Fig. S5e-f**). Of
188 those, 520 (28.6%) were nearby DAP-seq peaks, indicating that they are direct targets of SSP
189 and/or SSP2 (**Fig. 4g**). Clustering of the 520 putative direct targets revealed two main patterns of
190 gene expression that contained genes either down- or upregulated (de-repressed) in the *ssp^{CR}ssp2^{CR}*
191 double mutant (**Fig. 4h-i** and **Table S6**). Among the downregulated genes, we found both tomato

192 homologs of the Arabidopsis floral promoter *GI*, and a homolog of its interactor *FLAVIN-*
193 *BINDING, KELCH REPEAT, F-BOX 1 (FKF1)*²⁹. In addition, the MADS-box gene *SIMBP10*, a
194 homolog of the Arabidopsis floral promoter *FUL*, was downregulated in *ssp^{CR}ssp2^{CR}* double
195 mutants, while *SIMBP14* and a *FLOWERING LOCUS C (FLC)*-like gene were de-repressed in
196 *ssp^{CR}ssp2^{CR}*. We also identified several putative direct targets involved in phytohormone signaling.
197 Two cytokinin dehydrogenase/oxidase genes (*CKX1a, CKX5*) and putative negative regulators of
198 cytokinin levels were downregulated while a cytokinin activating enzyme encoding *SILONELY*
199 *GUYI (SILOG1)* gene was de-repressed in *ssp^{CR}ssp2^{CR}*. Furthermore, three abscisic acid receptor
200 genes (*PYLs*) were downregulated in the *ssp^{CR}ssp2^{CR}* double mutant. These data indicate that *SSP*
201 and *SSP2* redundantly regulate the expression of central regulators of the floral transition and
202 phytohormone responses, and guide meristem transitions towards floral fate.

203

204 ***SSP2* was lost during the evolution of *Physalis grisea*.** To determine whether genetic redundancy
205 between *SSP* and *SSP2* is evolutionary conserved, we inspected orthologs across eudicots (**Fig.**
206 **S6**). Surprisingly, our phylogenetic analyses indicated that tomato *SSP/SSP2* and Arabidopsis
207 *FD/FDP* resulted from independent duplication events in the *Solanaceae* and *Brassicaceae*
208 families (**Fig. S6**). When we inspected protein sequences of SSP-like transcription factors in the
209 *Solanaceae*, we identified a missense mutation in a conserved residue in the DNA-binding domain
210 of the potato SSP ortholog (**Fig. 2c**). Furthermore, we found only one SSP-like ortholog in *Physalis*
211 *grisea* (*PgSSP*; Phygri02g013770), a relative of tomato in the *Solanoideae* subfamily³⁰.
212 Phylogenetic and synteny analyses supported an evolutionary scenario in which the ortholog of
213 *SSP2* was lost in *P. grisea* (**Fig. 5a and Fig. S7a-c**). To obtain experimental evidence for the loss
214 of redundancy in *P. grisea*, we mutated *PgSSP* by CRISPR-Cas and quantified effects on shoot
215 architecture (**Fig. 5b**). Wild-type *P. grisea* plants produce seven leaves on the primary shoot before
216 terminating in a single-flowered inflorescence (**Fig. 5c**). Growth continues from two sympodial
217 meristems that each produce one sympodial unit, which results in a bifurcation of the shoot. Each
218 sympodial meristem produces two leaves and one flower, and in turn releases two additional
219 sympodial shoots. We observed alterations to this pattern in two independent *Pgssp^{CR}* mutant lines,
220 which produced an additional sympodial shoot at the first bifurcation and grew less compact than
221 the WT (**Fig. 5c, d-g**). The additional sympodial shoot on *Pgssp^{CR}* mutants resulted from a
222 sympodial meristem in the axil of an extra leaf that was produced before flowering, which

223 indicated that loss of *PgSSP* leads to a flowering delay (**Fig. 5e, h**). Together, these results suggest
224 that *PgSSP* regulates the transition of primary and sympodial meristems in the paralogue-free context
225 of *Physalis* in which *SSP2* is dispensable.

226

227 **Repairing *SSP2*^{F169} by base-editing in cultivated tomato leads to compact growth and earlier**
228 **yield.** Our findings in tomato show that *SSP2* acts partially redundant with *SSP* to promote the
229 transition to flowering on sympodial shoots (**Fig. 4a, d**). We asked whether restoring the activity
230 of *SSP2* in domesticated tomato by correcting the deleterious variant would accelerate the floral
231 transition. We tested this hypothesis by repairing the deleterious variant in domesticated tomato
232 by CRISPR-Cas base editing. The critical non-synonymous mutation results from a TCC (Ser) to
233 TTC (Phe) codon exchange (**Fig. 6a**). The correction of this mutation requires a A-to-G transition
234 on the reverse strand, which can be induced with an adenine base editor (ABE)³¹. Since none of
235 the nearby canonical PAMs (NGG) allowed us to position the target nucleotide into the high-
236 activity editing window (A4-A8) of the protospacer, we used the PAM-less Cas9 variant SpRY
237 fused to ABE8e (**Fig. 6a**)³². We edited *SSP2* in the domesticated and double-determinate S100
238 background³³ and observed high editing efficiency with edits at the target adenine in 37.5 % (3 of
239 8) second-generation (T1) transgenic families (**Fig. 6b** and **Fig. S8a**). In one T1 family we also
240 detected editing at the bystander T position (**Fig. S8a**). To determine whether the base-edited (be)
241 *ssp2*^{S169be} allele affected flowering time and shoot architecture, we generated segregating (F4)
242 populations and selected homozygous (*ssp2*^{S169be}/*ssp2*^{S169be}) and heterozygous (*ssp2*^{S169be}/*SSP*^{F169})
243 individuals for the repaired allele, and WT siblings (*SSP*^{F169}/*SSP*^{F169}) as controls by genotyping
244 (**Fig. 6c**). We found that plants homozygous or heterozygous for the repaired *ssp2*^{S169be} allele did
245 not flower earlier than their WT siblings (**Fig. 6d-e**). However, they developed less sympodial
246 shoot units and less flowers per inflorescence compared to WT siblings homozygous for the
247 domesticated (*SSP2*^{F169}) allele, which resulted in an overall more compact architecture (**Fig. 6d,f-**
248 **g**). To assess if repair of *SSP2* could compensate for the loss of *SSP*, we introduced the repaired
249 *ssp2*^{S169be} allele into the *ssp*^{CR} null mutant (in cv. S100). We found that *ssp2*^{S169be} did not suppress
250 late flowering and indeterminate growth of *ssp*^{CR} (**Fig. 6h-j**). However, we observed a partial and
251 significant suppression of late flowering on sympodial shoots (**Fig. 6h, k**). Moreover, *ssp*^{CR}
252 *ssp2*^{S169be} plants developed shorter inflorescences compared to *ssp*^{CR} mutants and WT (*SSP2*^{F169})

253 plants (**Fig. 6l**). Together, these results demonstrate that functional *SSP2* accelerates the
254 reproductive transition of meristems on sympodial shoots in partial redundancy with *SSP*.

255 Tomato production was revolutionized during the 20th century by the *self-pruning* mutation, which
256 confers determinate growth and facilitates mechanical harvesting. Our findings showed that a
257 functional *SSP2* allele accelerates sympodial shoot flowering and thus suggested an agronomic
258 value for this allele regarding earliness for yield. To test whether accelerated flowering from the
259 repaired *ssp2*^{S169be} allele leads to earlier yield, we quantified fruit production in segregating (F4)
260 populations under experimental greenhouse conditions (see **Online Methods**). We found that total
261 fruit yields, harvest index, and fruit size for *ssp2*^{S169be} plants were comparable to the WT sibling
262 controls (**Fig. 6n-o** and **Fig. S8b-e**). However, *ssp2*^{S169be} fruits had a reduced sugar content (brix)
263 (by 11%) (**Fig. S8f**). Notably, *ssp2*^{S169be} homozygotes displayed an 8% increase in the proportion
264 of ripe fruits compared to WT siblings, which was likely due to precocious flowering and
265 termination of sympodial shoots (**Fig. 6m, p**). Thus, compact growth from repairing the deleterious
266 *SSP2* mutation by base editing can confer earliness for fruit yields and represents a promising new
267 target for customizing tomato shoot architecture.

268

269 **DISCUSSION**

270 Here, we investigated the load of deleterious mutations that accumulated during domestication and
271 improvement of tomato. Within genes central to flowering time control, we discovered a
272 deleterious variant in the previously uncharacterized bZIP transcription factor gene *SSP2*. The
273 deleterious variant results in the exchange of a conserved serine to a phenylalanine in the DNA-
274 binding domain of the transcription factor. Our results from structural modelling, genome-wide
275 DNA binding assays, and genetic analyses indicate that the domesticated *SSP2*^{F169} variant partially
276 lost its ability to bind and regulate target genes that are largely shared between the ancestral
277 *SSP2*^{S169} variant and its paralog *SSP*. However, we cannot fully rule out that domesticated
278 *SSP2*^{F169} nonfunctionalized given its 353 private target genes and a subtle variation near the G-
279 box target motif. Interestingly, in the yeast bZIP factor Pap1, the equivalent serine-to-
280 phenylalanine exchange contributes to a similar change in binding specificity³⁴. Nevertheless, our
281 data shows that the deleterious variant in *SSP2* led to loss of genetic redundancy between *SSP* and
282 *SSP2*, a pair of paralogs that is widely conserved in flowering plants. In Arabidopsis, it was shown

283 that *FD* and *FDP* act redundantly during phytohormone responses while only *FD* affects the floral
284 transition, suggesting functional divergence of *FD*²¹. In contrast, our findings in tomato indicate
285 that *SSP* and *SSP2* act also partially redundant during the floral transition. Notably, our
286 phylogenetic analyses suggest that paralogs of *SSP* and *FD* arose independently in *Solanaceae* and
287 *Brassicaceae*, which could explain species-specific divergence of this paralogous pair. The
288 complete loss of a *PgSSP* paralog in *Physalis grisea* further supports dynamic evolution of the
289 paralog pair. Deleterious mutations and gene loss have been proposed as an important mechanism
290 of adaptation^{6,7}. However, the benefit of the deleterious *SSP2*^{F169} variant during domestication
291 remain speculative. Our genetic data demonstrates that domesticated *SSP2*^{F169} delays meristem
292 transitions on shoots and inflorescences. Notably, the domesticated *SSP2*^{F169} genotype develops
293 more flowers per inflorescence than the ancestral *SSP2*^{S169} genotype. Although flower number
294 correlates with fruit yield, the number of flowers per inflorescence in general decreased during
295 tomato domestication, likely due to source-sink imbalances driven by dramatic increases in fruit
296 size³⁵. This overall decrease in flower number during tomato domestication suggests that effects
297 from *SSP2*^{F169} on flower number were rather minor and difficult to select. Furthermore, the
298 deleterious *SSP2*^{F169} variant could have hitchhiked near QTLs that were selected during
299 domestication and improvement, which is a common scenario in crops with a narrow genetic base
300 such as tomato⁸. However, the closest known improvement sweep on chromosome 2 with five
301 fruit-weight QTLs is more than 5 Mbp away from *SSP2*, rendering linkage unlikely³⁶. Finally, we
302 cannot exclude that *SSP2*^{F169} is adaptive under specific conditions that were absent from our
303 experiments. Whether *SSP2*^{F169} was nearly fixed in cultivated tomato due to selection or drift
304 remains therefore an open question. Yet, the loss of genetic redundancy caused by a deleterious
305 mutation may reflect a common feature during the selection of crops in human-made
306 environments. The less-is-more idea proposes the accumulation of loss-of-function mutations as a
307 driver of rapid evolutionary change⁷, and gene loss may be even more frequent during the intense
308 artificial selection in domesticated environments. A reduced genetic repertoire in domesticated
309 genomes could result in lower genetic redundancy compared to their ancestral states and, as a
310 consequence, facilitate the exposure and selection of novel mutations, which are otherwise masked
311 by redundant paralogs. Our data shows that the ancestral *SSP2*^{S169} allele can suppress effects of
312 *ssp* mutations, which allow tuning of shoot architecture and optimization of tomato yields¹⁵.
313 Intriguingly, the deleterious *SSP2*^{F169} mutation, which broke redundancy with the paralog *SSP*,

314 may have been a prerequisite for the identification of the *ssp*²¹²⁹ breeding mutation. This illustrates
315 how standing variants can become adaptive due to genetic interactions with mutations that are
316 introduced or arose during breeding.

317 Correcting deleterious variants with genome editing in crops has been proposed as major strategy
318 for future crop breeding⁴. To our knowledge, we present here the first example of a direct repair
319 of a deleterious mutation in a crop using base editing. We show that repairing the deleterious *SSP2*
320 variant in tomato leads to precocious flowering on sympodial shoots and an overall more compact
321 plant architecture. Notably, precocious flowering and compact growth of base-edited plants was
322 associated with earliness for yield, with repaired plants displaying an 8% increase in ripe fruits at
323 harvest. Such earliness for fruit yield is a highly desirable trait for customizing shoot architecture
324 for specific environments. Our work shows that base editing provides a promising approach for
325 correcting deleterious variants that accumulated during domestication and improvement in crops.
326 However, our study also emphasizes that deleterious mutations are not unfavorable *per se* and may
327 have adaptive roles that are only exposed in specific genetic backgrounds or environmental
328 conditions.

329

330 **FIGURE LEGENDS**

331

332 **Figure 1: Predicting the load of deleterious variants along the domestication history of**
333 **tomato. a**, Number of predicted deleterious mutations in a panel of 82 tomato genomes, including
334 wild species (*S. pimpinellifolium*, green), landraces (*S. lycopersicum* var. *cerasiforme*, orange),
335 and cultivars (*S. lycopersicum*, purple). **b-c**, Prediction of deleterious variants across all CETS (b)
336 and Group-A bZIP (c) genes. The dashed red line indicates the threshold for deleterious prediction
337 (SIFT-score<0.05). Dot size scales with the number of genomes that carry the variant. Red font
338 indicates genes with predicted deleterious mutations.

339

340 **Figure 2: A deleterious mutation in SSP2 reduces its transcription factor activity. a**,
341 Maximum-likelihood tree of A-group bZIP proteins in tomato (red font) and Arabidopsis (blue
342 font). Red arrowhead marks SSP2. Numbers represent bootstrap values from 1,000 replicates and
343 scale bar indicates the average number of substitutions per site. **b**, Normalized gene expression
344 (TPM) for *SSP* and *SSP2* in different tissues and developmental stages (veg. earl./mid./late, stand
345 for early, middle and late vegetative meristem stage). **c**, Partial alignment of SSP-like bZIP
346 proteins from Arabidopsis, domesticated tomato (*S. lycopersicum*; *Slyc*), close wild tomato relative
347 (*S. pimpinellifolium*; *Spim*), distant wild tomato relative (*S. pennellii*; *Spen*), potato (*S. tuberosum*;
348 *St*), and *Physalis grisea* (*Pg*). Red arrowheads mark conserved DNA-binding residues. **d**,
349 Distribution of ancestral (*SSP2*^{S169}) and derived (*SSP2*^{F169}) *SSP2* alleles in distant wild tomato
350 relatives, wild relatives (*S. galapagense* / *S. cheesmaniae*), wild progenitor species (*S.*
351 *pimpinellifolium*), landraces (*S. lyc* var. *cerasiforme*), and cultivars (*S. lycopersicum*). n=number
352 of accessions. **e**, Predicted structures of ancestral *SSP2*^{S169} and derived *SSP2*^{F169} proteins on target
353 DNA determined by homology modelling. Insets show a magnified view of the
354 serine/phenylalanine residue at position 169. **f**, Reporter assays in tobacco leaves using *SSP*,
355 *SSP2*^{F169}, and *SSP2*^{S169} as effectors and firefly Luciferase (fLuc) driven by upstream sequences of
356 *MC* (*pMC::fLUC*), *SIFUL1* (*pSIFUL1::fLUC*), and *SIFUL2* (*pSIFUL1::fLUC*) as reporter.
357 Numbers indicate technical replicates. Ctrl indicates no effector control. Letters represent post-hoc
358 Tukey's HSD tests results with 95% confidence level.

359 **Figure 3: Domesticated SSP2^{F169} shows reduced binding at genome-wide target loci.** **a,**
360 Overlap of significant ($\log_2FC \geq 3$, $FDR \leq 0.01$) SSP, SSP2^{F169}, and SSP2^{S169} DAP-seq peaks
361 ($n=14'091$). **b,** Distribution of significant SSP, SSP2^{F169}, and SSP2^{S169} DAP-seq peaks across gene
362 features. **c,** Most-significant motifs identified by *de-novo* motif enrichment analysis of SSP,
363 SSP2^{F169}, and SSP2^{S169} DAP-seq peak regions. Grey box delimits region with motif variation
364 outside the core-motif. **d,** Overlap of genes with significant DAP-seq peaks ≤ 3 Kbp upstream and
365 ≤ 2 Kbp downstream of the transcriptional start site ($n=7'114$). **e,** Profiles of normalized read
366 coverage at significant SSP, SSP2^{F169}, and SSP2^{S169} peaks. **f,** Comparison of SSP, SSP2^{F169}, and
367 SSP2^{S169} DAP-seq peaks relative to the transcriptional start (TSS) and end (TES) site of nearby
368 genes ($n=7'114$). **g-h,** Browser view of SSP, SSP2^{F169}, and SSP2^{S169} DAP-seq peaks at
369 *SIGIGANTEA-LIKE1* (g) and *SIGIGANTEA-LIKE2* (h). Normalized coverage (CPM) is shown in
370 yellow, green and blue. Significant peak regions are indicated by red boxes.

371

372 **Figure 4: SSP and SSP2 act partially redundant to regulate the transition to flowering.** **a,**
373 Representative images of wild-type S100, *spp*^{CR} and *spp2*^{CR} single mutants, and *spp spp2*^{CR} double
374 mutants. L= leaf number, arrowheads mark the last leaf before flowering. Determinate (D) and
375 indeterminate (ID) shoots are indicated. Scale bars represent 7.5 cm. **b,** Schematic depiction of
376 tomato shoot architecture. Different shades of green delimit primary and sympodial shoots. **c-e,**
377 Quantification of the floral transition (number of leaves before flowering) on the primary (c) and
378 secondary (d) shoots, and the number of flowers per inflorescence (e) for genotypes shown in (a).
379 The number of plants (c,d) and inflorescences (e) are indicated. Letters represent post-hoc Tukey's
380 HSD tests results with 95% confidence level. **f,** Principal component analysis of 22'726 expressed
381 genes in transition meristems of the WT, *spp*, *spp2*, and *spp spp2*, determined by RNA-seq. **g,**
382 Overlap of genes differentially expressed ($\log_2FC \geq 0.58$, $FDR \leq 0.05$) in *spp*, *spp2*, and/or *spp*
383 *spp2* with genes at SSP, SSP2^{F169}, and SSP2^{S169} DAP-seq peaks. **h,** Heatmap depicting expression
384 of 520 putative SSP/SSP2 target genes. **i,** Normalized expression levels for selected putative direct
385 targets. Genes are color coded based on the biological pathway.

386

387 **Figure 5: The genome of *Physalis grisea* encodes a single direct SSP ortholog that regulates**
388 **meristem transitions.** **a,** Scheme of the phylogenetic tree of tomato and closely related

389 *Solanaceae* species. Filled circles, empty circles or star show presence, absence, or missense
390 mutation, respectively, of *SSP/SSP2* or *FD/FDP* in these species. Full tree is displayed in Fig. S6.
391 **b**, CRISPR-Cas9 targeting of *PgSSP* in *P. grisea*. Blue boxes, black lines, and grey boxes represent
392 exonic, intronic, and untranslated regions, respectively. Single guide RNAs (sgRNAs) are
393 indicated with red arrowheads. PAM and sgRNA sequences are indicated in black and red bold
394 letters, respectively; deletions are indicated with blue dashes; sequence gap length is given in
395 parenthesis. Insertions are indicated by blue letters. **c**, Model of the growth habit of *P. grisea* WT
396 and *Pgssp^{CR}* plants. Different shades of green delimit primary, first sympodial, and second
397 sympodial shoots. The color of leaves corresponds with the shoot of origin. Note that the last leaf
398 of each shoot is displaced upwards during shoot development. **d**, Representative pictures
399 illustrating the difference in number of sympodial shoots in WT and *Pgssp* mutant plants. Last leaf
400 before the shoot bifurcation is indicated (L5). White arrowheads indicate individual sympodial
401 shoots. Scale bar represents 7.5 cm. **e**, Representative stereoscope images of the shoot apex of WT
402 and *Pgssp* mutant plants. Upper images show the apex with a terminal flower (*). Lower images
403 show the same view with the flower removed. The sympodial meristems (SYMs) are delimited by
404 a dashed line and numbered in developmental order. Scale bar represents 100 μ m. **f-h**,
405 Quantification of the number of sympodial shoots at the first and second bifurcation, and flowering
406 time (number of leaves before the first inflorescence). Number of plants is indicated at the bottom
407 of the plots. Letters represent post-hoc Tukey's HSD tests results with 95% confidence level.

408

409 **Figure 6: Repairing the deleterious *SSP2* mutation in domesticated tomato by base-editing**
410 **leads to compact growth and earliness for yield. a**, Base-editing strategy to correct the
411 deleterious *SSP2* mutation in domesticated tomato using an adenosine base editor (ABE) and a
412 PAM-less Cas9 variant. The target adenine in *SSP2* (A5) is at position 5 of the protospacer with a
413 bystander adenine (A6) at position 6. Editing of the target codon (TTC) can lead to three different
414 outcomes depending on which adenine is deaminated. Only editing the target nucleotide (A5)
415 alone reverts the phenylalanine codon (TTC) back to the ancestral serine (TCC). **b**, Validation of
416 editing in a chimeric first-generation (T0) transgenic and the corresponding T1 progeny by Sanger
417 sequencing. The target nucleotide is indicated by a red arrowhead. **c**, Crossing scheme to generate
418 the segregating *ssp2^{S169be}* F4 population. **d**, Representative pictures showing the total number of
419 sympodial units on WT and *ssp2^{S169be}* plants. Terminal inflorescences of each sympodial unit are

420 indicated by a white arrow. **e-g**, Quantification of flowering time (number of leaves before the first
421 inflorescence), number of sympodial shoots, and number of flowers per truss of WT, $ssp2^{S169be/+}$
422 and $ssp2^{S169be}$ plants. **h**, Representative pictures showing the number of leaves per sympodial unit
423 and determinacy of WT, ssp^{CR} , $ssp^{CR} ssp2^{S169be/+}$ and $ssp^{CR} ssp2^{S169be}$ plants. **i-l**, Quantification of
424 flowering time (as in (e)), number of determinate plants, number of leaves per sympodial unit
425 (SU), and number of flowers per truss of WT, ssp^{CR} , $ssp^{CR} ssp2^{S169be/+}$ and $ssp^{CR} ssp2^{S169be}$ plants.
426 Determinate (D) and indeterminate (ID) shoots are indicated. **m**, Representative images showing
427 the full harvest of individual WT, $ssp2^{S169be/+}$ and $ssp2^{S169be}$ plants. Percentage of red fruits is
428 indicated. **n-p**, Quantification of total fruit yield (n), harvest index (total fruit yield / plant weight)
429 (o), and percentage of red fruits. Number of plants are indicated in the plots for (e-g), (i-k) and (l-
430 o). Letters on top of the plots represent post-hoc Tukey's HSD tests results with 95% confidence
431 level. Scale bars represent 10 cm (d) and 7.5 cm in (h,m).

432

433 **SUPPLEMENTARY FIGURE LEGENDS**

434

435 **Figure S1: Prediction of deleterious variants in tomato. a**, Number of coding sequence variants
436 across a panel of 82 genomes. **b**, Number of non-synonymous variants predicted to be tolerated
437 (sift-score ≥ 0.05), deleterious (sift-score < 0.05), or without prediction (na). Color code indicates
438 confidence of SIFT prediction. **c**, Number of heterozygous and homozygous predicted deleterious
439 mutations in wild (*S. pimpinellifolium*, n=27, in green), landrace (*S. lyc. var. cerasiforme*, n=23,
440 in orange), and domesticated (*S. lycopersicum*, n=32, in purple) tomato genomes.

441

442 **Figure S2: Phylogenetic analysis of the bZIP transcription factor family in Arabidopsis and**
443 **tomato.** Maximum-likelihood phylogenetic tree constructed with full-length bZIP protein
444 sequences from Arabidopsis (n=74) and tomato (n=70). Arabidopsis and tomato proteins are
445 indicated in black and red font, respectively. The yeast protein Pap1 was used as an outgroup (blue
446 font). Proteins were classified into 13 groups (A-K, M, S) according to the Arabidopsis
447 nomenclature³⁷. Numbers represent bootstrap values from 1000 replicates, and scale bar indicates
448 the average number of substitutions per site.

449

450 **Figure S3: Introgression of ancestral *SSP2*^{SI69} into domesticated tomato suppresses late**
451 **flowering and indeterminate growth of *spp* mutants. a**, Representative image of greenhouse-
452 grown wild-type (WT) and *SSP2*^{SI69}-NIL individual in the determinate M82 background. **b-d**,
453 Quantification of the floral transition (the number of leaves before flowering) on primary (b) and
454 sympodial shoots (c), and the number of sympodial shoot units (d). **e, f**, Representative images of
455 field-grown WT and *SSP2*^{SI69}-NIL plants at flowering (e) and fruiting (f) stage. **g**, Representative
456 images of detached WT, *spp*²¹²⁹ and *spp*²¹²⁹ *SSP2*^{SI69}-NIL shoots (in the determinate M82
457 background). D, determinate; ID, indeterminate; L, leaves. **h**, Quantification of the floral transition
458 on the primary shoot for genotypes shown in (e). Numbers at the bottom and letters at the top of
459 the plots of (b) and (f) represent the number of replicate plants and post hoc Tukey's HSD test
460 results with 95% confidence level, respectively. Scale bars indicate 10 cm (a, e, f) and 1 cm (g).

461

462 **Figure S4: Identification of SSP, SSP2^{F169}, and SSP2^{S169} genome-wide binding sites by DAP-**
463 **seq. a,** Overlap of SSP, SSP2^{F169}, and SSP2^{S169} DAP-seq peaks at different significant thresholds
464 ($\log_2FC \geq 2, 3, 4$). **b,** Distribution of SSP, SSP2^{F169}, and SSP2^{S169} DAP-seq peaks across gene
465 features at different significant thresholds as in (a) **c,** Profiles of normalized read coverage at SSP,
466 SSP2^{F169}, and SSP2^{S169} peaks at different significant thresholds as in (a). **d,** Overlap of genes with
467 DAP-seq peaks ≤ 3 Kbp upstream and ≤ 2 Kbp downstream of the transcriptional start site, at
468 different significant thresholds as in (a). **e,** Comparison of SSP, SSP2^{F169}, and SSP2^{S169} DAP-seq
469 peaks relative to the transcriptional start (TSS) and end (TES) site of nearby genes, at different
470 significant thresholds as in (a). Top and bottom panels show coverage profiles and heatmaps,
471 respectively.

472

473 **Figure S5: Targeting SSP and SSP2 in two tomato cultivars by CRISPR-Cas9. a,b** CRISPR-
474 Cas9 targeting of *SSP* and *SSP2* in *S. lycopersicum* cv. S100 (a) and cv. M82 (b). Orange boxes,
475 black lines, and grey boxes represent exonic, intronic, and untranslated regions, respectively.
476 Single guide RNAs (sgRNAs) are indicated with red arrowheads. PAM and protospacer sequences
477 are indicated in black and red bold letters, respectively; deletions are indicated with blue dashes;
478 sequence gap length is given in parenthesis. **c,** Representative images WT S100, *ssp*^{CR} and *ssp2*^{CR}
479 single mutants, and *ssp ssp2*^{CR} double mutants. L= leaf number, white arrowheads mark
480 inflorescences. Determinate (D) and indeterminate (ID) shoots are indicated. Scale bars represents
481 1 cm. **d,** Quantification of the floral transition on the primary shoot for genotypes in (c). N, number
482 of plants. Letters represent post hoc Tukey's HSD tests. **e,** Volcano plots showing differentially
483 expressed genes ($\log_2 FC > 0.58, FDR < 0.05$) in *ssp*^{CR} and *ssp2*^{CR} single mutants, and *ssp ssp2*^{CR}
484 double mutants compared to WT (cv. M82). **f,** Heatmap of z-scores showing expression pattern
485 for 1'832 genes that are differentially expressed ($\log_2 FC > 0.58, FDR < 0.05$) in *ssp*^{CR}, *ssp2*^{CR}
486 single mutants, and/or *ssp ssp2*^{CR} double mutants in M82.

487

488 **Figure S6: Phylogenetic analysis of SSP homologs in eudicots.** Maximum-likelihood
489 phylogenetic tree constructed with 128 full-length bZIP protein sequences from 51 eudicot species.
490 Tomato, Arabidopsis, and Physalis proteins are highlighted in red, blue, and orange font,
491 respectively. Red branches indicate duplication events, and the two separate duplication events in

492 the *Solanaceae* and *Brassicaceae* are highlighted with stars. Numbers represent bootstrap values
493 from 1000 replicates, and scale bar indicates the average number of substitutions per site.

494

495 **Figure S7: The ortholog of *SSP2* in *Physalis grisea* was lost during evolution.** **a.** Maximum-
496 likelihood phylogenetic tree of the group A bZIP transcription factor family of *A. thaliana*, *S.*
497 *lycopersicum* and *P. grisea*. Numbers represent bootstrap values from 1000 replicates, and scale
498 bar indicates the average number of substitutions per site. **b,c,** Browser view of synteny analysis
499 of *SSP* (b) and *SSP2* (c) between tomato (cv. S100) and *P. grisea*. Yellow rectangles show
500 annotated genes and yellow streaks link them with their syntenic counterpart. *SSP* and *SSP2* genes
501 are indicated in red. Note the lack of a unique syntenic block for *SSP2* in *P. grisea* in (c).

502

503 **Figure S8: Base-editing of *SSP2* in domesticated tomato and its effect on different tomato**
504 **yield components.** **a,** CRISPR base-editing sequencing result of three T0 individuals (upper row)
505 and their T1 progeny (lower row). Note that the target edit was detected in only one T0 individual
506 (T0-3) but in three T1 families. One T1 individual (T1-9-17) was also edited at the bystander
507 adenine. The edited nucleotides are indicated by a red arrowhead. **b-f,** Quantification of the
508 vegetative biomass (b), total red and green fruit harvest (c,d), average fruit weight (e), and average
509 soluble sugar content (brix) (f). The number of plants are indicated in the plots. Letters on top of
510 the plots represent post-hoc Tukey's HSD tests results with 95% confidence level.

511

512

513 **SUPPLEMENTARY TABLES**

514 Table S1: List of accessions for deleterious variant analyses

515 Table S2: Number of predicted deleterious variants

516 Table S3: SIFT-score predictions for non-synonymous variants in CETS and Group-A bZIP genes

517 Table S4: List of significant SSP and SSP2 DAP-seq peaks

518 Table S5: List of genes associated with significant SSP and SSP2 DAP-seq peaks

519 Table S6: List of putative SSP/SSP2 target genes

520 Table S7: Assembly statistics

521 Table S8: List of primers used in this study

522 Table S9: List of gRNA sequences used in this study

523

524 **ONLINE METHODS**

525 Plant material, growth conditions, and phenotyping

526 Seeds of *S. lycopersicum* cv. M82 (LA3475), *S. lycopersicum* cv. Sweet-100 (S100) double-
527 determinate³³, *S. pimpinellifolium* (LA1589), *P. grisea*, and *N. benthamiana* were from our own
528 stocks. Tomato seeds were directly sown and germinated in soil in 96-cell plastic flats. The
529 *P.grisea* seeds were incubated at 48°C for 3 days prior to sowing to increase germination rates.
530 Plants were grown under long-day conditions (16-h light/ 8-h dark) in a greenhouse under natural
531 light supplemented with artificial light from high-pressure sodium bulbs (~250umol m⁻²s⁻¹).
532 Temperature was 25°C and relative humidity was 50-60%. Plants were grown in 5L pots (2 plants
533 per pot) under drip irrigation and standard fertilizer regimes. Tomato plants were pruned and only
534 the primary shoot and the proximal axillary shoot were kept. Phenotypic data was collected from
535 the F3 and T4 generation for *ssp^{CR} ssp2^{CR}* plants in the S100 background, the F7 (*ssp^{CR}* and *ssp2^{CR}*)
536 and F4 (*ssp^{CR} ssp2^{CR}*) generation in the M82 background, and the T3 generation for *PgSSP^{CR}* in
537 *Physalis* and the F4 generation in *ssp ssp2^{S169be}* plants. Data for flowering time sympodial shoot
538 number, per sympodial shoot, and number of flowers per inflorescence were collected from the
539 primary shoot and the proximal shoot. To assess different tomato yield components under
540 experimental greenhouse conditions, mature plants were harvested 79 days after transplanting. For
541 data collection, plants and fruits were manually removed from the soil and the plant, respectively.
542 The total fruit yield was defined as the sum of red and green fruits from each plant. The harvest
543 index was calculated by dividing the total fruit yield by the plant weight (i.e., the vegetative
544 biomass after the removal of fruits). Ten fruits from each plant were randomly selected to measure
545 average fruit weight and total soluble sugar content (brix) in fruit juice. Brix was quantified using
546 a digital Brix refractometer (HANNA® instruments, HI96801). All statistical analyses of
547 phenotyping data were conducted in R³⁸.

548 *N. benthamiana* (tobacco) seeds were directly sown on soil in square pots. Seedlings were grown
549 under long-day conditions (16-h light/ 8-h dark) in a plant growth room under LED light panels
550 (~100umol m⁻²s⁻¹) and constant temperature (22°C). Approximately one week after germination,
551 tobacco seedlings were singled out into individual square pots and grown for an additional 2-3
552 weeks before leaf infiltration.

553

554 LA1589 de novo genome assembly

555 Nanopore long read sequences for the *S. pimpinellifolium* accession LA1589 were previously
556 generated^{16,39}. Basecalling was performed using Guppy v3.1.5. Illumina sequencing data were
557 previously generated²⁴. We assembled the Nanopore and Illumina sequences together with
558 MaSuRCA (v3.4.1)⁴⁰. The resulting contigs were then scaffolded against the Heinz 4.0 reference
559 genome using RaGOO (v1.1)⁴¹. Gaps were closed with LR_Gapcloser (v3)⁴² and the assembly was
560 polished with 3 rounds of Pilon (v1.23)⁴³. Assembly statistics can be found in **Table S7**. We used
561 liftOff⁴⁴ to annotate the LA1589 assembly with ITAG4.0 gene models and tomato pan-genome
562 genes as previously described³³.

563

564 Genome-wide prediction of deleterious variants

565 Illumina raw reads from 27 *S. pimpinellifolium* and 28 *S. lycopersicum* accessions (**Table S1**) were
566 retrieved from public repositories as described before⁴⁵ (Gao et al). Reads were aligned to the *S.*
567 *pimpinellifolium* reference genome (LA1589v0.1) using BWA-MEM (v0.7.17) using default
568 parameters. Alignments were sorted and duplicates marked with PicardTools (v2.26.2) and
569 indexed using samtools (v1.15.1)⁴⁶. Variants were called with bcftools (v.1.15.1, parameters
570 mpileup --no-BAQ --ignore-RG -d 1000000 -Q0 --annotate FORMAT/AD,FORMAT/DP).
571 Variants were filtered with vcftools (v0.1.14, parameters --min-alleles 2 --max-alleles 2 --minQ
572 30 --minDP 5 --maxDP 50 --mac 2 --recode --recode-INFO-all). Filtered variant call format (vcf)
573 files were then used to predict deleterious mutations using SIFT-4G¹⁷. A custom SIFT library was
574 built from the *S. pimpinellifolium* reference genome sequence (SpimLA1589_v0.1) and annotation
575 (SolpimLA1589_v0.2) using the SIFT instructions and default parameters. The LA1589 SIFT
576 library contained SIFT scores for 70% of genes (21578 of 30808), SIFT scores for 83% of positions
577 (56424493/67919880), and confident scores for 73% of positions (41083097/56424493). SIFT
578 was used to determine the effect of coding sequence variants on protein sequence, and to predict
579 deleterious missense variants. Variant types and SIFT scores were plotted in R using the ggplot2
580 package.

581

582 Phylogenetic analyses and sequence alignments

583 Protein sequences of tomato and Arabidopsis bZIP family members were obtained from the Plant
584 Transcription Factor Database (PlantTFDB, v5.0)⁴⁷. Physalis bZIP protein sequences were
585 identified in a BLAST search on the Phygr1.3.1 protein annotation³⁰ using the SSP protein
586 sequence as query. Full-length amino acid sequences of 70 tomato, 74 Arabidopsis, 58 Physalis,
587 and yeast Pap1 (SPAC1783.07c.1) bZIP proteins were aligned using MAFFT (v7.481) using
588 default parameters⁴⁸. Maximum likelihood phylogenetic trees were constructed in IQ-Tree
589 (v2.2.0.5; parameters -m MFP -bb 1000 -bnni -redo)⁴⁹ and visualized in FigTree (v1.4.4;
590 <http://tree.bio.ed.ac.uk/software/figtree/>). Average number of substitutions per site are indicated
591 by the scale bars. Specific bZIP groups were assigned according to their Arabidopsis homologs³⁷.

592 To reconstruct the phylogenetic tree of the bZIP family in eudicots we used the OMA browser's⁵⁰
593 July 2023 release to collect a pool of homologs for tree building. The Hierarchical Orthologous
594 Groups (HOGs) were identified by searching for the tomato SSP gene's identifier
595 (Solyc02g083520) for the initial HOG and then adding additional closely related HOGs, inferred
596 to be closely related as they share many predicted orthologs. The following HOGs were
597 downloaded: D0228852, D0178917, D0181214, D0210160, D0214417, D0216285, D0223413
598 (accessed 23 Jan 2024). Additionally, through BLAST searches, we incorporated the bZIP gene of
599 *Amborella trichopoda* and closely related bZIP genes from eight *Solanaceae* species: *Nicotiana*
600 *benthamiana*, *Nicotiana tabacum*, *Phylloscopus griseolus*, *Petunia axillaris*, *Petunia inflata*,
601 *Solanum tuberosum*, *Capsicum annum*, and *Capsicum chinense*. The final dataset comprised 128
602 genes from 51 plant species. These protein sequences were aligned using the approach described
603 in the PhylomeDB pipeline⁵¹. Briefly, we obtained alignments in forward and reverse directions
604 using three programs (MUSCLE v3.8.1551⁵², MAFFT v7.490⁴⁸, and Kalign v3.3.5⁵³). Then, the
605 six alignments were combined using M-COFFEE v13.46.0.919e8c6b⁵⁴. The phylogenetic tree was
606 reconstructed using a maximum likelihood approach as implemented in IQ-TREE v2.2.2.6⁵⁵, using
607 the best-fit model identified by ModelFinder⁵⁶ (JTT+F+I+R5) and 1000 ultrafast bootstrap
608 replicates. The tree was manually rooted using *Amborella trichopoda* as the outgroup. Duplication
609 events were inferred using ETE v4.0⁵⁷ using the species overlap method⁵⁸.

610

611 Homology modelling

612 The HHpred server was used to find suitable templates for SSP2 protein modeling⁵⁹. The final
613 templates were chosen based on the sequence similarity in the area of protein-DNA interaction,
614 not on the highest sequence identity to the target.

615 The 50 homology models of wild tomato protein SSP2^{S169} dimers were calculated using Modeller
616 9v18²⁵ and CCAAT/enhancer-binding protein beta (C/EBP beta) as a template. The crystal
617 structure of human C/EBP beta in complex with DNA is stored under 1HJB code in the Protein
618 Data Bank²⁶. The target and template sequence shared 26% of sequence identity. The best model
619 in term of its DOPE score⁶⁰ was chosen.

620 Analogically, the 50 homology models of domestic tomato SSP2^{F169} protein dimers were
621 calculated based on the structure of Pap1 transcription factor as a template and the best model,
622 according to DOPE score, was chosen. The crystal structure of Pap1 factor is stored in the PDB
623 under 1GD2 code and shares 24% of sequence identity with the SSP2F169 protein³⁴. For both
624 SSP2 proteins the DNA molecule from the template structure was included in the models. The
625 DNA sequence was changed to the SSP2 recognition motif with UCSF Chimera tool that was also
626 used for visualization of the models⁶¹.

627

628 Molecular cloning

629 Binary vectors for CRISPR-Cas9 mutagenesis in domesticated tomato were assembled using the
630 Golden Gate cloning system as previously described^{33,62}. For CRISPR-Cas9 mutagenesis in *S.*
631 *pimpinellifolium* and Sweet-100, a new Level (L) 1 part pICH47742_SpCas9-P2A-GFP was
632 cloned by amplifying the coding sequence of SpCas9 from pICH47742::35S::Cas9 (Addgene no.
633 49771) using primers P94 and P129. The fragments were cloned into the L0 acceptor pAGM1287
634 to generate pAGM1287-SpCas9. P2A-GFP was amplified from pGG-D-P2A-GFP-NLS-E⁶³ using
635 primer P96 and P97 and cloned into the L0 acceptor pAGM1301 to generate pAGM1301_P2A-
636 GFP. The pAGM1287_SpCas9 and pAGM1301_P2A-GFP parts were combined with pICH51288
637 (2Xp35S) and pICH41421 (nosT) in pICH47742 (L1 acceptor) to generate pICH47742_SpCas9-
638 P2A-GFP. For CRISPR-Cas base editing, the PAM-less adenosine base editor ABE8e-SpRY³²
639 was domesticated by amplifying four fragments using the primer pairs P576/ P577, P578/ P579,
640 P580/ P581, P582/P583 on the template pYPQ262B³². Fragments were cloned into the L-1
641 acceptor pAGM1311 and combined in the L0 acceptor pAGM1287 to generate

642 pAGM1287_ABE8e-SpRY. pAGM1287_ABE8e-SpRY was combined with pAGM1301_P2A-
643 GFP, pICH51288 (2Xp35S), and pICH41421 (nosT) in the L1 acceptor pICH47742 to generate
644 pICH47742_SpRY-ABE8e-P2A-GFP. Constructs for transactivation assays were cloned using the
645 Golden Gate MoClo kit⁶². The p19 construct for silencing suppression was assembled with the L1
646 acceptor pICH47742 and the L0 parts pICH85281 (pMas), pICH44022 (p19), and pICH77901
647 (tMas). The YFP construct was assembled with the L1 acceptor pICH47742 and the L0 parts
648 pICH51266 (p35S), pICSL80014 (YFP), and pICH41414 (t35S). To clone the SFT co-effector and
649 the SlycSSP2 effector constructs, the coding sequences of SFT and SlycSSP2 were amplified from
650 *S. lycopersicum* (cv. M82) transition meristem cDNA with gene specific primer pairs (SFT:
651 SFT_F/SFT_R, SlycSSP2: SSP2_F/SSP2_R). To clone the SpimSSP2 effector construct, the
652 coding sequence of SpimSSP2 was amplified from *S. pimpinellifolium* (LA1589) transition
653 meristem cDNA with the primer pair SSP2_F/SSP2_R. The amplicons were cloned into the L0
654 acceptor pICH41308. To clone SSP effector construct, the coding sequences of SSP2 was
655 amplified from *S. lycopersicum* (cv. M82) transition meristem cDNA in two fragments with the
656 primer pairs SSP_F1/SSP_R1 and SSP_F2/SSP_R2 and cloned into the L-1 acceptor pAGM1311.
657 The L-1 parts were cloned into the L0 acceptor pICH41308. Individual L0 effector parts (SSP,
658 SlycSSP2, and SpimSSP2) were combined with pICSL13001 (p35S), pICSL30009 (Myc-tag), and
659 pICH41414 (t35S) in the L1 acceptor pICH47772. The L0 co-effector part (SFT) was combined
660 with pICSL13001 (p35S), pICSL30008 (HA-tag) and pICH41414 (t35S) in the L1 acceptor
661 pICH47761. To clone the luciferase reporter constructs, the upstream regions of pMC, pFUL, and
662 pFUL2 were amplified from *S. lycopersicum* (cv. M82) gDNA in multiple fragments gene-specific
663 primer pairs (pMC: pMC_F1/pMC_R1 and pMC_F2/pMC_R2; pFUL1: pFUL1_F3/pFUL1_R3
664 pFUL1_F2p/FUL1_R2p, and FUL1_F1/pFUL1_R1; pFUL2: pFUL2_F1/pFUL2_R1 and
665 pFUL2_F2/pFUL2_R2) and cloned into the L-1 acceptor pAGM1311. The pMC construct
666 contained 2170 bp genomic sequence including upstream region, the 5'UTR, and the first exon.
667 The pFUL1 and pFUL2 constructs contained 2640 bp and 2040 bp genomic sequence,
668 respectively, including upstream regions and the 5'UTR. The L-1 parts were cloned into the L0
669 acceptor pICH41295. Individual L0 effector parts (pMC, pFUL1, and pFUL2) were combined
670 with pICSL80001 (fLuc) and pICH41432 (tOCS) in the L1 acceptor pICH47751. All primers and
671 gRNA sequences used for cloning are listed in **Table S8 and S9**.

672

673 CRISPR/Cas9 genome editing, plant transformation and identification of mutant alleles

674 CRISPR-Cas9 mutagenesis in tomato and physalis was performed as described previously^{33,64,65}.
675 Briefly, guide RNAs (gRNAs) were designed using the CRISPOR tool and the M82v1.0, Sweet-
676 100v2.0 or Phygriv1.0 genome assemblies. Final vectors were transformed into the tomato cultivar
677 M82, LA1589 or double-determinate Sweet-100, or into *P. grisea* by *Agrobacterium tumefaciens*-
678 mediated transformation. CRISPR-Cas9 editing in tomato and physalis was verified by genotyping
679 or amplicon sequencing as described³³. Base editing was quantified in first-generation (T0)
680 transgenics using EditR v1.0.10⁶⁶ and in the T1 generation with a CAPS marker. All primer
681 sequences are listed in **Table S8**.

682

683 Generation of near-isogenic lines (NILs)

684 Near-isogenic *SSP2^{SI69}* lines in the domesticated M82 background were generated by crossing the
685 *S. pimpinellifolium* accession LA1589 with *S. lycopersicum* cv. M82), and backcrossing F2
686 individuals homozygous for *SSP2^{SI69}* to the recurrent parent (*S. lyc.* cv. M82) over 4 (BC4) to 5
687 (BC5) generations. Presence *SSP2^{SI69}* allele was confirmed by genotyping using a CAPS marker
688 (**Table S8**).

689

690 Transactivation assays

691 Transient transactivation assays with luciferase reporter constructs were conducted in *N.*
692 *benthamiana* leaves as previously described⁶⁷. In brief, leaves of 3-4 week old plants were
693 infiltrated with mixtures of *A. tumefaciens* (strain GV3101) cultures containing effector, co-
694 effector, luciferase reporter, transfection control, and silencing inhibitor vectors. Effector
695 constructs contained the coding sequence (CDS) of *SSP*, *SSP2^{F169}* or *SSP2^{SI69}* with an N-terminal
696 Myc tag and driven by the CaMV 35S promoter. The co-effector construct contained the CDS of
697 *SFT* with an N-terminal HA tag and driven by CMV 35S promoter. The luciferase reporter
698 constructs contained the CDS of fLUC driven by the upstream regions of *MC*, *SIFUL*, or *SIFUL2*.
699 The transfection control was pGREENII-0800-LUC, which contains the CDS of rLUC driven by
700 the CMV 35S promoter. A p19 construct was used to suppress silencing. Liquid cultures were
701 grown in 4 ml LB in 15 mL round-bottom Falcon tubes for 36 hrs at 30°C and 220 rpm.

702 Agrobacteria were harvested by centrifugation at 3000 rpm and resuspended in infiltration buffer
703 (50 mM MES pH 5.7 and 10 mM MgCl₂) to an OD₆₀₀ = 1. Before leaf infiltration, individual
704 cultures were incubated up to 3 hrs at RT and combined to obtain mixtures with effectors, reporters
705 (fLUC), and transfection control (pGREEN 35S:rLUC), and silencing inhibitor (p19) plasmids at
706 final OD₆₀₀ of 0.1, 0.1, 0.1, and 0.05. Agrobacteria mixtures were infiltrated into the 5th leaf using
707 a needleless syringe, with four to twelve different plants being infiltrated for each combination.
708 Leaf disks of 0.8 cm diameter were harvested 3 days after infiltration and flash-frozen in liquid
709 nitrogen before grinding in a mix mill (twice 15 s⁻¹ for 30s). Luciferase assays were performed
710 using the Dual-Luciferase Reporter Assay System (Promega) and a Tecan Sapphire plate reader. In
711 short, leaf powder was extracted in 300 µl of 1x PLB and vigorously vortexed for 30 s. Volumes
712 of 10 µl protein extracts were mixed with 40 µl luciferase reagent in 96-well microplates and
713 incubated for 10 min at RT. Firefly luciferase (fLUC) activity was quantified with a 10 s
714 integration time. Afterwards, reactions were mixed with 30 µl Stop & Glo and incubated for 10
715 min before Renilla luciferase (rLUC) activity was measured with a 10 s integration time.
716 Transactivation activity of the effectors was determined by calculating the fLUC/rLUC ratios and
717 statistically significant differences were determined using one-factor ANOVAs followed by Tukey
718 tests.

719

720 DAP-seq

721 Myc-tagged coding sequences of *SSP*, *SSP2^{F169}* and *SSP2^{S169}* were amplified from effector
722 constructs used in the transactivation assay. The pTnT™ vector, and the *SSP2^{F169}* and *SSP2^{S169}*
723 inserts were digested using XhoI (NEB) and NotI-HF (NEB) and combined using T4 Ligase
724 (NEB). The Myc-tagged coding sequence for *SSP* was amplified from M82 cDNA and cloned into
725 pTnT™ vectors with the NEBuilder HiFi DNA Assembly Cloning Kit (NEB #E5520). Plasmid
726 DNA was isolated from 100 ml bacterial cultures using the PureYield™ Plasmid Midiprep System
727 (Promega, A2492). Two replicates of *SSP* and *SSP2* proteins were expressed *in-vitro* in the TnT®
728 SP6 High-Yield Wheat Germ Protein Expression System (Promega, L3260) from 3.5 µg plasmid
729 DNA per reaction. High molecular weight DNA for genomic library construction was isolated
730 from inflorescence meristem tissue of the *anantha* mutant in the Sweet-100 genotype using a
731 CTAB protocol as described previously³³. DAP-seq was performed as previously described with

732 minor modifications^{27,68}. The DNA-library was prepared according to Franco-Zorilla & Prat
733 (2021) with minor modifications. The gDNA library was purified using SPRI beads (B23317,
734 Beckman Coulter). Adaptor ligation was verified by qPCR with primers specific for the indices
735 (**Table S8**) and the KAPA standards 20, 2 and 0.2 nM (Roche) in 10 µl reaction volumes. DNA
736 affinity-purification steps were performed according to Bartlett et al. (2017) with 75 ng of gDNA
737 input library per replicate. Eluted libraries were single-indexed (**Table S8**). Eight uniquely indexed
738 libraries were produced, two replicate libraries per protein (SSP, SSP2^{F169}, SSP2^{S169}) and two
739 replicates of the input library as negative control. Indexed libraries were purified individually with
740 the Monarch® PCR & DNA Cleanup Kit (NEB, T1030S). Individual indexed libraries were
741 analyzed on a Fragment Analyzer (Agilent), purified with SPRI beads and pooled at equimolar (10
742 nM) concentrations. The pooled libraries were sequenced on 1 Illumina NovaSeq6000 lane at the
743 Genome Technology Facility (GTF) of the University of Lausanne. A total of 753'327'838 PE150
744 reads (between 64'808'988 and 144'444'123 per sample) were generated.

745 Raw read quality was assessed using FastQC (v0.11.9;
746 <http://www.bioinformatics.babraham.ac.uk/projects/fastqc/>). Adapter sequences were trimmed
747 with NGmerge (v0.3, parameters -g -d -a)⁶⁹. Reads were aligned to the SollycSweet-100v2.0
748 reference³³ with hisat2 (v2.2.0, default parameters)⁷⁰, and alignments were sorted and indexed
749 using samtools (v1.15.1)⁴⁶. Differential binding (DB) analysis was performed with the
750 Bioconductor csaw package (v1.301)⁷¹. We used a window width of 10 bp and an estimated
751 fragment length of 213 bp. Prior to counting, repeats were blacklisted from the genome using the
752 SollycSweet-100v2.0 TE annotation³³. To filter regions and windows, we used the global
753 enrichment approach of the csaw module. Bins of 10000 bp were used for global background
754 estimation. The median of the average abundances across all 10000 bp bins was used as the global
755 background coverage estimate. We only retained windows with at least a 4-fold change from the
756 global background coverage. We counted the reads into large bins and normalized with the
757 wrapper function normFactors, which uses trimmed mean of M-values (TMM) method. Significant
758 regions were identified with the csaw makeContrasts function (FDR ≤0.01). Gene-based
759 annotation of differentially-bounds regions was performed using the detailRanges function of csaw
760 (3 Kbp upstream and 2 Kbp downstream of TSS) and annotation file SollycSweet-
761 100_genes_v2.1.1.gff3³³. BED files with significant regions and BigWig files with normalized
762 read coverage were exported via the *export* function of the rtracklayer package⁷² in R. *De-novo*

763 motif discovery was performed with the 1000 most significant peaks (by FDR) for each sample by
764 analysing genomic sequences from position -100 to +100 relative to the peak center using MEME
765 (v 5.3.3; parameters -dna -mod zoops -nmotifs 3 -minw 6 -maxw 15 -maxsites 1000 -objfun classic
766 -revcomp -markov_order 0)⁷³.

767 Genome-wide distribution of peaks was determined using CHIPSeeker (v1.32.0)⁷⁴ by annotating
768 regions +/- 5 Kbp around the TSS with the function annotatePeak (parameters tssRegion=c(-5000,
769 5000)). Peak intensity profiles and peak heatmaps were generated using the computeMatrix,
770 plotHeatmap, and plotProfile functions in deepTools⁷⁵. The most-enriched motifs for SSP,
771 SSP2^{F169}, and SSP2^{S169} were mapped to the SollycSweet-100v2.0 reference³³ with the FIMO tool
772 of the MEME Suite⁷³. Browser shots of peak coverage, peak regions and binding motifs at putative
773 direct targets were generated in jbrowse2⁷⁶.

774

775 RNA-seq

776 Meristem staging, collection, RNA extraction, and library construction for the *ssp*^{CR-181} (188 bp
777 deletion allele), *ssp2*^{CR-122} (122 bp deletion allele) and *ssp*^{CR-181}*ssp2*^{CR-122} mutants, and the WT in
778 the genetic background of cv. M82 was performed as previously described²³. In brief, seedlings
779 shoot apices were collected at the transition (TM) stage of meristem maturation, and immediately
780 submerged in ice-cold acetone. Shoot apices were manually dissected under a stereoscope and
781 three biological replicates consisting of 14-22 meristems were collected per genotype from
782 individual seedlings. Total RNA was extracted with the Arcturus Pico-Pure RNA Extraction kit
783 (Thermo). We prepared indexed libraries using the TruSeq Stranded mRNA Library Prep kit from
784 Illumina according to the manufacturer's instructions. Fragment size and concentration were
785 assessed with a Bioanalyzer. Libraries were sequenced on 2 Illumina NovaSeq6000 lanes at the
786 Genome Technology Facility (GTF) of the University of Lausanne. A total of 187'907'134 SE100
787 reads (between 14'133'226 and 17'789'680 per sample) were generated.

788 The quality of raw reads was assessed using FastQC (v0.11.9;
789 <http://www.bioinformatics.babraham.ac.uk/projects/fastqc/>). Raw reads were aligned to the
790 genome reference M82v1.0³³ using STAR⁷⁷ (v2.7.6a; parameters --runMode alignReads --
791 outFilterType BySJout --outFilterMultimapNmax 20 --outMultimapperOrder Random --
792 alignSJoverhangMin 8 --alignSJDBoverhangMin 1 --alignIntronMin 20 --alignIntronMax

793 1000000 --alignMatesGapMax 1000000). Alignments were sorted and indexed using samtools⁴⁶
794 and gene expression was quantified as unique read pairs aligned to reference annotated gene
795 features (M82v1.1.1) using HTSeq-count (v0.11.2; parameter --order=pos --stranded=no --
796 type=exon --idattr=Parent)⁷⁸.

797 All statistical analyses of gene expression were conducted in R³⁸. Differentially expressed genes
798 (DEGs) between the mutants *ssp*, *ssp2*, *ssp ssp2*, and the WT were determined with DESeq2
799 (v1.34.0)⁷⁹. Raw count data was transformed in DESeq2 by variant stabilizing transformation
800 (VST). Reproducibility of biological replicates was assessed by hierarchical clustering (method
801 ward.D) and principle component analysis (PCA) using the PCAtools package (v2.6.0) in R³⁸.
802 Significantly differentially expressed genes (DEGs) were identified in *ssp* (n=686), *ssp2* (n=180),
803 and *sspssp2* (n=1507) genes with a 1.5-fold change ($\log_2FC \geq 0.58$, compared to the WT) and
804 adjusted *p*-value ≤ 0.05 cutoff. Gene normalized z-scores were visualized in heatmaps using
805 pheatmap (v1.10.12) and normalized expression of individual transcripts in transcripts per million
806 (TPM) was plotted using ggplot2.

807

808 DATA AVAILABILITY

809 The LA1589 genome assembly is available at the Solanaceae Genomics Network
810 (https://solgenomics.net/ftp/genomes/Solanum_pimpinellifolium/LA1589/2020/). Raw Nanopore
811 sequence data is available on SRA under the BioProjects PRJNA607731 and PRJNA557253. Raw
812 Illumina sequence data will be made available on SRA under the BioProject PRJNA1069353 upon
813 publication. Seeds are available on request from S. Soyk.

814

815 ACKNOWLEDGEMENTS

816 We thank all members of the Soyk lab, Y. Eshed, and C. Fankhauser for helpful discussions; J.
817 Marquis and J. Weber for support with sequencing; B. Tissot, L. Nerny, V. Vashanthakumar, Y.
818 Emmenegger, A. Chatillon, L. Keel, and T. Stupp for support with plant care; G. Ghazi Soltani
819 and S. Mainiero for support with experiments; J. M. Franco-Zorrilla for advice with DAP-seq; J.
820 van Eck and K. Swartwood for advice with plant transformation; Z. Lippman, Y. Qi, and T. Jacobs
821 for providing materials. This work was supported by the University of Lausanne, the European

822 Research Council (ERC) under the European Union’s Horizon 2020 research and innovation
823 programme (ERC Starting Grant “EPICROP” Grant No. 802008) to S.So., the Swiss National
824 Science Foundation (SNSF) under an Eccellenza Professorial Fellowship (Grant No.
825 PCEFP3_181238) and Project Grant (Grant No. 310030_212218) to S.So., and an UNIL
826 Interdisciplinary Project Grant to N.Gl. and S.So., and an National Science Foundation Grant
827 (IOS-1546625) to G.B.M and S.St..

828

829 **AUTHOR CONTRIBUTIONS**

830 A.N.G., S.St., and S.So. conceived the project and designed and planned experiments

831 A.N.G., M.B, L.L., J.I., I.J., J.Z., S.So. performed experiments and collected data

832 A.N.G., M.B, J.I., G.A., I.J., J.Z., R.R., C.I., N.Gu., J.J.-G., N.Gl., S.St., S.So. analysed data

833 N.Gl., G.B.M., S.St., S.So. aquired project funding.

834 A.N.G. and S.So. wrote the first draft of the manuscript

835 All authors read, edited, and approved the manuscript.

836

837 **REFERENCES**

- 838 1. Koenig, D. *et al.* Comparative transcriptomics reveals patterns of selection in domesticated
839 and wild tomato. *Proc Natl Acad Sci U S A* **110**, E2655–E2662 (2013).
- 840 2. Renaut, S. & Rieseberg, L. H. The Accumulation of Deleterious Mutations as a
841 Consequence of Domestication and Improvement in Sunflowers and Other Compositae
842 Crops. *molecubar biology evolution* **32**, 2273–2283 (2015).
- 843 3. Moyers, B. T., Morrell, P. L. & McKay, J. K. Genetic Costs of Domestication and
844 Improvement. *Journal of Heredity* **109**, 103–116 (2018).
- 845 4. Wallace, J. G., Rodgers-Melnick, E. & Buckler, E. S. On the Road to Breeding 4.0:
846 Unraveling the Good, the Bad, and the Boring of Crop Quantitative Genomics. *Annual*
847 *reviews genetics* **52**, 421–444 (2018).
- 848 5. Zhang, C. *et al.* The genetic basis of inbreeding depression in potato. *Nat Genet* **51**, 374–
849 378 (2019).
- 850 6. Monroe, J. G., McKay, J. K., Weigel, D. & Flood, P. J. The population genomics of adaptive
851 loss of function. *Heredity (Edinb)* **126**, 383–395 (2021).
- 852 7. Olson, M. V. MOLECULAR EVOLUTION '99 When Less Is More: Gene Loss as an
853 Engine of Evolutionary Change. *Am. J. Hum. Genet* **64**, 18–23 (1999).
- 854 8. Gao, C. Genome engineering for crop improvement and future agriculture. *Cell* **184**, 1621–
855 1635 (2021).
- 856 9. Gaarslev, N., Swinnen, G. & Soyk, S. Meristem transitions and plant architecture—learning
857 from domestication for crop breeding. *Plant Physiol* 1–12 (2021)
858 doi:10.1093/plphys/kiab388.
- 859 10. Shalit, A. *et al.* The flowering hormone florigen functions as a general systemic regulator
860 of growth and termination. *Proceedings of the National Academy of Sciences* **106**, 8392–
861 8397 (2009).
- 862 11. Lifschitz, E., Ayre, B. G. & Eshed, Y. Florigen and anti-florigen – a systemic mechanism
863 for coordinating growth and termination in flowering plants. *Front Plant Sci* **0**, 465 (2014).

- 864 12. Lifschitz, E. & Eshed, Y. Universal florigenic signals triggered by FT homologues regulate
865 growth and flowering cycles in perennial day-neutral tomato. *J Exp Bot* **57**, 3405–3414
866 (2006).
- 867 13. Zhu, Y. *et al.* TERMINAL FLOWER 1-FD complex target genes and competition with
868 FLOWERING LOCUS T. *Nature Communications* 2020 11:1 **11**, 1–12 (2020).
- 869 14. Taoka, K. I. *et al.* 14-3-3 proteins act as intracellular receptors for rice Hd3a florigen. *Nature*
870 **476**, 332–335 (2011).
- 871 15. Park, S. J. *et al.* Optimization of crop productivity in tomato using induced mutations in the
872 florigen pathway. *Nat Genet* **46**, 1337–1342 (2014).
- 873 16. Alonge, M. *et al.* Major Impacts of Widespread Structural Variation on Gene Expression
874 and Crop Improvement in Tomato. *Cell* **182**, 145–161 (2020).
- 875 17. Vaser, R., Adusumalli, S., Ngak Leng, S., Sikic, M. & Ng, P. C. SIFT missense predictions
876 for genomes. *Nat Protoc* **11**, 1073–1081 (2016).
- 877 18. Soyk, S. *et al.* Variation in the flowering gene SELF PRUNING 5G promotes day-neutrality
878 and early yield in tomato. *Nature Genetics* 2016 49:1 **49**, 162–168 (2017).
- 879 19. Rodríguez-Leal, D., Lemmon, Z. H., Man, J., Bartlett, M. E. & Lippman, Z. B. Engineering
880 Quantitative Trait Variation for Crop Improvement by Genome Editing. *Cell* **171**, 470-
881 480.e8 (2017).
- 882 20. Abe, M. *et al.* FD, a bZIP protein mediating signals from the floral pathway integrator FT
883 at the shoot apex. *Science (1979)* **309**, 1052–1056 (2005).
- 884 21. Romera-Branchat, M. *et al.* Functional Divergence of the Arabidopsis Florigen-Interacting
885 bZIP Transcription Factors FD and FDP. *Cell Rep* **31**, 107717 (2020).
- 886 22. Wigge, P. A. *et al.* Integration of spatial and temporal information during floral induction
887 in Arabidopsis. *Science (1979)* **309**, 1056–1059 (2005).
- 888 23. Park, S. J., Jiang, K., Schatz, M. C. & Lippman, Z. B. Rate of meristem maturation
889 determines inflorescence architecture in tomato. *Proceedings of the National Academy of*
890 *Sciences* **109**, 639–644 (2012).

- 891 24. Consortium, T. T. G. The tomato genome sequence provides insights into fleshy fruit
892 evolution. *Nature* **485**, 635–641 (2012).
- 893 25. Šali, A. & Blundell, T. L. Comparative Protein Modelling by Satisfaction of Spatial
894 Restraints. *J Mol Biol* **234**, 779–815 (1993).
- 895 26. Tahirov, T. H. *et al.* Structural analyses of DNA recognition by the AML1/Runx-1 Runt
896 domain and its allosteric control by CBFbeta. *Cell* **104**, 755–767 (2001).
- 897 27. Bartlett, A. *et al.* Mapping genome-wide transcription-factor binding sites using DAP-seq.
898 *Nat Protoc* **12**, 1659–1672 (2017).
- 899 28. Fowler, S. *et al.* GIGANTEA: a circadian clock-controlled gene that regulates
900 photoperiodic flowering in Arabidopsis and encodes a protein with several possible
901 membrane-spanning domains. *EMBO J* **18**, 4679–4688 (1999).
- 902 29. Sawa, M., Nusinow, D. A., Kay, S. A. & Imaizumi, T. FKF1 and GIGANTEA complex
903 formation is required for day-length measurement in Arabidopsis. *Science (1979)* **318**, 261–
904 265 (2007).
- 905 30. He, J. *et al.* Establishing Physalis as a Solanaceae model system enables genetic
906 reevaluation of the inflated calyx syndrome. *Plant Cell* **35**, 351–368 (2023).
- 907 31. Richer; Michelle F. *et al.* Phage-assisted evolution of an adenine base editor with improved
908 Cas domain compatibility and activity. *Nature Biotechnology* **38**, 883–891 (2020).
- 909 32. Ren, Q. *et al.* PAM-less plant genome editing using a CRISPR–SpRY toolbox. *Nat Plants*
910 **7**, 25–33 (2021).
- 911 33. Alonge, M. *et al.* Automated assembly scaffolding using RagTag elevates a new tomato
912 system for high-throughput genome editing. *Genome Biol* **23**, 258 (2022).
- 913 34. Fujii, Y., Shimizu, T., Toda, T., Yanagida, M. & Hakoshima, T. Structural basis for the
914 diversity of DNA recognition by bZIP transcription factors. *Nat Struct Biol.* **10**, 889–893
915 (2000).
- 916 35. Grandillo, S. & Tanksley, S. D. *QTL Analysis of Horticultural Traits Differentiating the*
917 *Cultivated Tomato from the Closely Related Species Lycopersicon Pimpinellifolium.* *Theor*
918 *Appl Genet* vol. 92 (1996).

- 919 36. Lin, T. *et al.* Genomic analyses provide insights into the history of tomato breeding. *Nat*
920 *Genet* **46**, 1220–1226 (2014).
- 921 37. Dröge-Laser, W., Snoek, B. L., Snel, B. & Weiste, C. The Arabidopsis bZIP transcription
922 factor family — an update. *Curr Opin Plant Biol* **45**, 36–49 (2018).
- 923 38. R Core Team. R: A language and environment for statistical computing. Preprint at (2021).
- 924 39. Wang, X. *et al.* Genome of *Solanum pimpinellifolium* provides insights into structural
925 variants during tomato breeding. *Nat Commun* **11**, (2020).
- 926 40. Zimin, A. V *et al.* Genome analysis The MaSuRCA genome assembler. *Bioinformatics* **29**,
927 2669–2677 (2013).
- 928 41. Alonge, M. *et al.* RaGOO: Fast and accurate reference-guided scaffolding of draft genomes.
929 *Genome Biol* **20**, 1–17 (2019).
- 930 42. Xu, G. C. *et al.* LR_Gapcloser: a tiling path-based gap closer that uses long reads to
931 complete genome assembly. *Gigascience* **8**, 1–14 (2019).
- 932 43. Walker, B. J., Abeel, T. ♂, Shea, T., Priest, M. & Abouelliel, A. Pilon: An Integrated Tool
933 for Comprehensive Microbial Variant Detection and Genome Assembly Improvement.
934 *PLoS One* **9**, 112963 (2014).
- 935 44. Shumate, A. & Salzberg, S. L. Liftoff: accurate mapping of gene annotations.
936 *Bioinformatics* **37**, 1639–1643 (2021).
- 937 45. Gao, L. *et al.* The tomato pan-genome uncovers new genes and a rare allele regulating fruit
938 flavor. *Nat Genet* **51**, 1044–1051 (2019).
- 939 46. Li, H. *et al.* The Sequence Alignment/Map format and SAMtools. *Bioinformatics* **25**, 2078–
940 2079 (2009).
- 941 47. Jin, J. *et al.* PlantTFDB 4.0: toward a central hub for transcription factors and regulatory
942 interactions in plants. *Nucleic Acids Res* **45**, D1040–D1045 (2017).
- 943 48. Katoh, K. & Standley, D. M. MAFFT Multiple Sequence Alignment Software Version 7:
944 Improvements in Performance and Usability. *Mol Biol Evol* **30**, 772–780 (2013).

- 945 49. Minh, Q. B. *et al.* IQ-TREE 2: New Models and Efficient Methods for Phylogenetic
946 Inference in the Genomic Era. *Molecular Biology and Evolution* **37**, 1530–1534 (2020).
- 947 50. Altenhoff, A. M. *et al.* OMA orthology in 2024: improved prokaryote coverage, ancestral
948 and extant GO enrichment, a revamped synteny viewer and more in the OMA Ecosystem.
949 *Nucleic Acids Res* **52**, 513–521 (2024).
- 950 51. Huerta-Cepas, J. *et al.* PhylomeDB v3.0: an expanding repository of genome-wide
951 collections of trees, alignments and phylogeny-based orthology and paralogy predictions.
952 *Nucleic Acids Res* **39**, D556–D560 (2011).
- 953 52. Edgar, R. C. MUSCLE: multiple sequence alignment with high accuracy and high
954 throughput. *Nucleic Acids Res* **32**, 1792–1797 (2004).
- 955 53. Lassmann, T. & Sonnhammer, E. L. L. Kalign - An accurate and fast multiple sequence
956 alignment algorithm. *BMC Bioinformatics* **6**, 1–9 (2005).
- 957 54. Wallace, I. M., O’Sullivan, O., Higgins, D. G. & Notredame, C. M-Coffee: combining
958 multiple sequence alignment methods with T-Coffee. *Nucleic Acids Res* **34**, 1692–1699
959 (2006).
- 960 55. Minh, B. Q. *et al.* IQ-TREE 2: New Models and Efficient Methods for Phylogenetic
961 Inference in the Genomic Era. *Mol Biol Evol* **37**, 1530–1534 (2020).
- 962 56. Kalyaanamoorthy, S., Minh, B. Q., Wong, T. K. F., Von Haeseler, A. & Jermini, L. S.
963 modelfinder: fast model selection for accurate phylogenetic estimates. *Nat Methods* **14**,
964 (2017).
- 965 57. Huerta-Cepas, J., Serra, F. & Bork, P. ETE 3: Reconstruction, Analysis, and Visualization
966 of Phylogenomic Data. *Mol Biol Evol* **33**, 1635–1638 (2016).
- 967 58. Huerta-Cepas, J., Dopazo, H., Dopazo, J. & Gabaldón, T. The human phylome. *Genome*
968 *Biol* **8**, 1–16 (2007).
- 969 59. Gabler, F. *et al.* Protein Sequence Analysis Using the MPI Bioinformatics Toolkit. *Curr*
970 *Protoc Bioinformatics* **72**, e108 (2020).
- 971 60. Shen, M. & Sali, A. Statistical potential for assessment and prediction of protein structures.
972 *Protein Sci* **15**, 2507 (2006).

- 973 61. Pettersen, E. F. *et al.* UCSF Chimera—A visualization system for exploratory research and
974 analysis. *J Comput Chem* **25**, 1605–1612 (2004).
- 975 62. Engler, C., Youles, M. & Gruetzner, R. A Golden Gate Modular Cloning Toolbox for
976 Plants. *ACS Synth Biol* **3**, 839–843 (2014).
- 977 63. Decaestecker, W. *et al.* CRISPR-TSKO: A Technique for Efficient Mutagenesis in Specific
978 Cell Types, Tissues, or Organs in Arabidopsis. *Plant Cell* **31**, 2868–2887 (2019).
- 979 64. Swartwood, K., Joyce, · & Eck, V. Development of plant regeneration and Agrobacterium
980 tumefaciens-mediated transformation methodology for *Physalis pruinosa*. *Plant Cell Tissue*
981 *Organ Cult* **137**, 465–472 (2019).
- 982 65. Brooks, C., Nekrasov, V., Lippman, Z. B. & Van Eck, J. Efficient gene editing in tomato
983 in the first generation using the clustered regularly interspaced short palindromic
984 repeats/CRISPR-associated9 system. *Plant Physiol* **166**, 1292–1297 (2014).
- 985 66. Kluesner, M. G. *et al.* EditR: A Method to Quantify Base Editing from Sanger Sequencing.
986 *CRISPR J* **1**, 239 (2018).
- 987 67. Galvão, V. C. *et al.* PIF transcription factors link a neighbor threat cue to accelerated
988 reproduction in Arabidopsis. *Nat Commun* **10**, 1–10 (2019).
- 989 68. Franco-Zorrilla, J. M. & Prat, S. DAP-Seq Identification of Transcription Factor-Binding
990 Sites in Potato. in *Methods in Molecular Biology* vol. 2354 123–142 (Humana Press Inc.,
991 2021).
- 992 69. Gaspar, J. M. NGmerge: Merging paired-end reads via novel empirically-derived models of
993 sequencing errors. *BMC Bioinformatics* **19**, 1–9 (2018).
- 994 70. Kim, D., Paggi, J. M., Park, C., Bennett, C. & Salzberg, S. L. Graph-based genome
995 alignment and genotyping with HISAT2 and HISAT-genotype. *Nature Biotechnology* **2019**
996 *37:8* **37**, 907–915 (2019).
- 997 71. Lun, A. T. L. & Smyth, G. K. csaw: a Bioconductor package for differential binding analysis
998 of ChIP-seq data using sliding windows. *Nucleic Acids Res* **44**, 45 (2015).
- 999 72. Lawrence, M., Gentleman, R. & Carey, V. rtracklayer: an R package for interfacing with
1000 genome browsers. *BIOINFORMATICS APPLICATIONS NOTE* **25**, 1841–1842 (2009).

- 1001 73. Bailey, T. L., Johnson, J., Grant, C. E. & Noble, W. S. The MEME Suite. *Nucleic Acids Res*
1002 **43**, 39–49 (2015).
- 1003 74. Yu, G., Wang, L.-G. & He, Q.-Y. ChIPseeker: an R/Bioconductor package for ChIP peak
1004 annotation, comparison and visualization. *Bioinformatics* **31**, 2382–2383 (2015).
- 1005 75. Ramírez, F., Dündar, F., Diehl, S., Grüning, B. A. & Manke, T. deepTools: a flexible
1006 platform for exploring deep-sequencing data. *Nucleic Acids Res* **42**, W187–W191 (2014).
- 1007 76. Diesh, C. *et al.* JBrowse 2: a modular genome browser with views of synteny and structural
1008 variation. *Genome Biol* **24**, 1–21 (2023).
- 1009 77. Dobin, A. *et al.* STAR: ultrafast universal RNA-seq aligner. *Bioinformatics* **29**, 15–21
1010 (2013).
- 1011 78. Anders, S., Pyl, P. T. & Huber, W. HTSeq—a Python framework to work with high-
1012 throughput sequencing data. *Bioinformatics* **31**, 166–169 (2015).
- 1013 79. Love, M. I., Huber, W. & Anders, S. Moderated estimation of fold change and dispersion
1014 for RNA-seq data with DESeq2. *Genome Biol* **15**, 1–21 (2014).
- 1015
- 1016

Figure 1

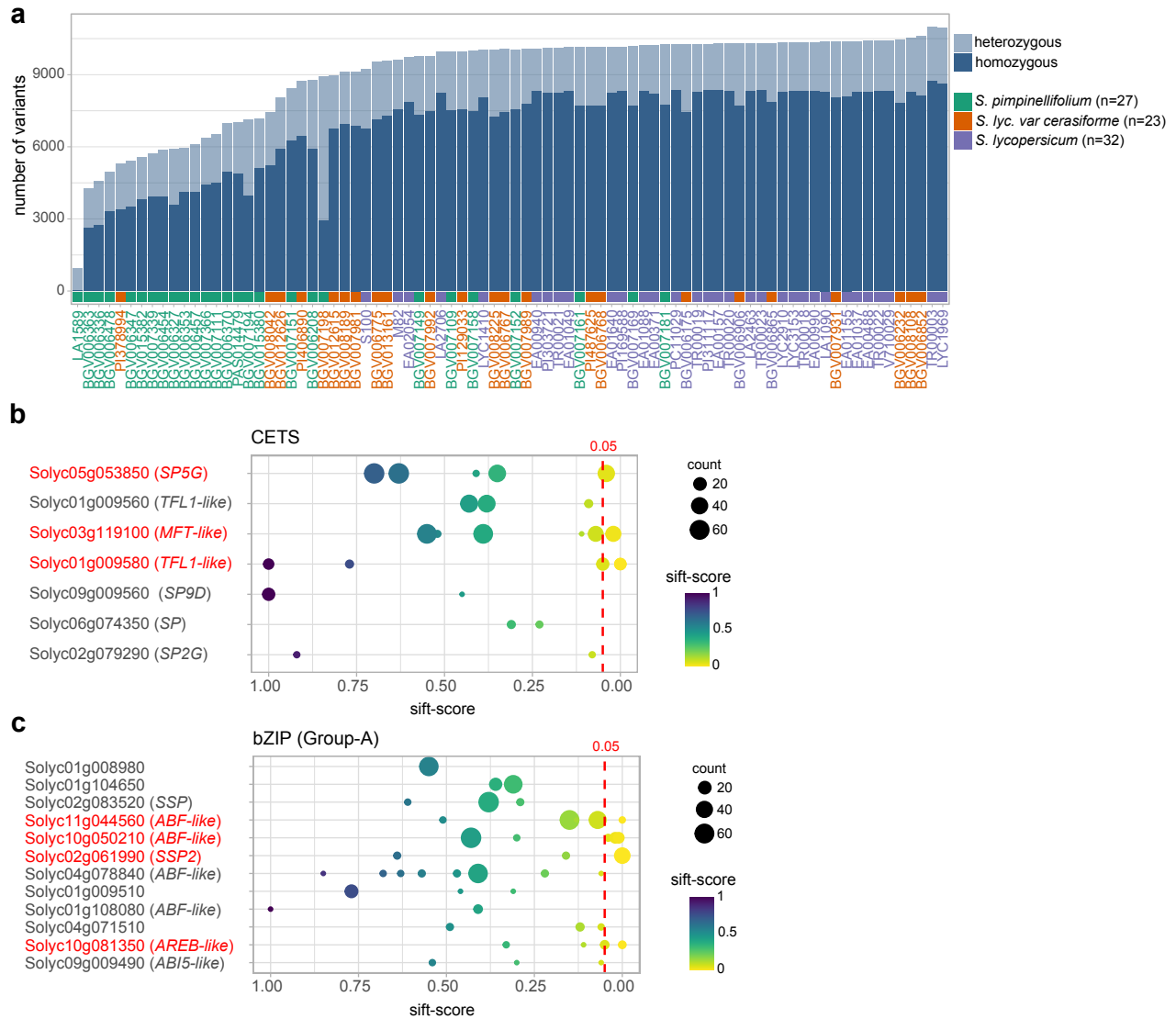


Figure 1: Predicting the load of deleterious variants along the domestication history of tomato. a, Number of predicted deleterious mutations in a panel of 82 tomato genomes, including wild species (*S. pimpinellifolium*, green), landraces (*S. lycopersicum* var. *cerasiforme*, orange), and cultivars (*S. lycopersicum*, purple). **b-c,** Prediction of deleterious variants across all CETS (b) and Group-A bZIP (c) genes. The dashed red line indicates the threshold for deleterious prediction (SIFT-score<0.05). Dot size scales with the number of genomes that carry the variant. Red font indicates genes with predicted deleterious mutations.

Figure 2

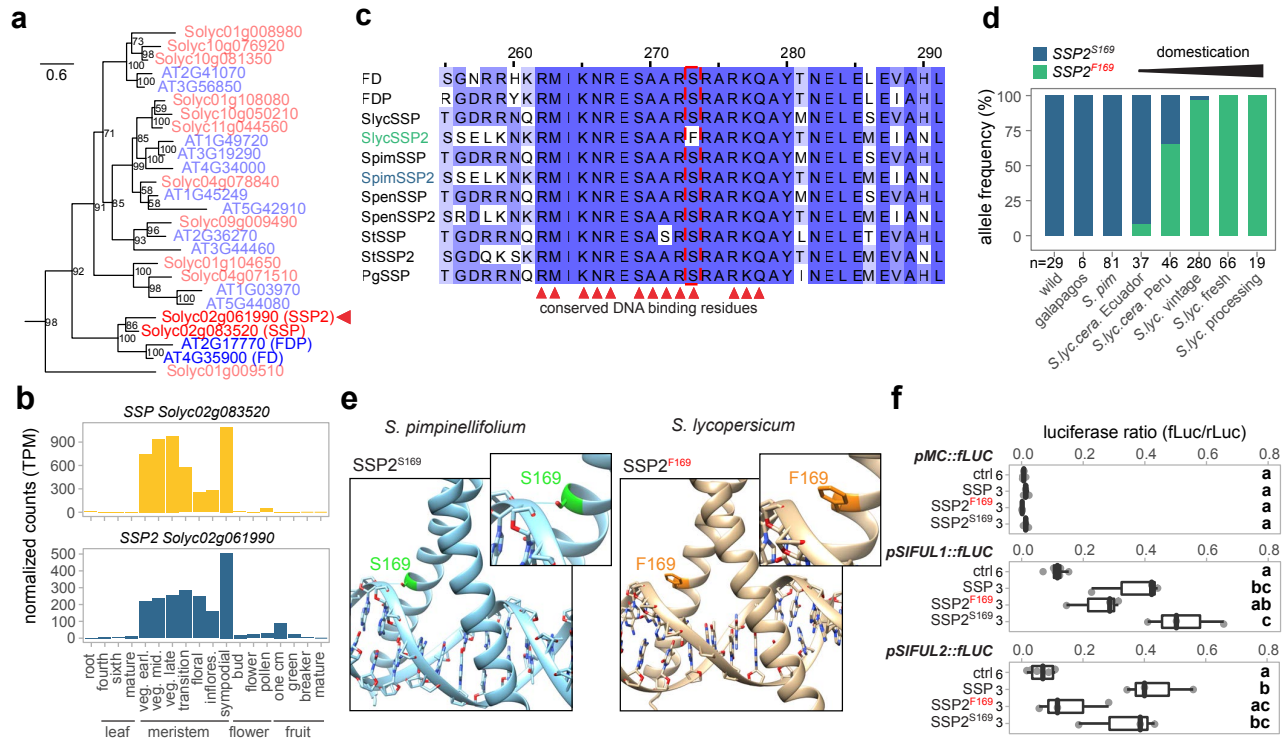


Figure 2: A deleterious mutation in *SSP2* reduces its transcription factor activity. **a**, Maximum-likelihood tree of A-group bZIP proteins in tomato (red font) and Arabidopsis (blue font). Red arrowhead marks *SSP2*. Numbers represent bootstrap values from 1,000 replicates and scale bar indicates the average number of substitutions per site. **b**, Normalized gene expression (TPM) for *SSP* and *SSP2* in different tissues and developmental stages (veg. earl./mid./late, stand for early, middle and late vegetative meristem stage). **c**, Partial alignment of *SSP*-like bZIP proteins from Arabidopsis, domesticated tomato (*S. lycopersicum*; *Slyc*), close wild tomato relative (*S. pimpinellifolium*; *Spim*), distant wild tomato relative (*S. pennellii*; *Spen*), potato (*S. tuberosum*; *St*), and *Physalis grisea* (*Pg*). Red arrowheads mark conserved DNA-binding residues. **d**, Distribution of ancestral (*SSP2*^{S169}) and derived (*SSP2*^{F169}) *SSP2* alleles in distant wild tomato relatives, wild relatives (*S. galapagense* / *S. cheesmaniae*), wild progenitor species (*S. pimpinellifolium*), landraces (*S. lyc* var. *cerasiforme*), and cultivars (*S. lycopersicum*). n=number of accessions. **e**, Predicted structures of ancestral *SSP2*^{S169} and derived *SSP2*^{F169} proteins on target DNA determined by homology modelling. Insets show a magnified view of the serine/phenylalanine residue at position 169. **f**, Reporter assays in tobacco leaves using *SSP*, *SSP2*^{F169}, and *SSP2*^{S169} as effectors and firefly Luciferase (fLuc) driven by upstream sequences of *MC* (*pMC::fLUC*), *SIFUL1* (*pSIFUL1::fLUC*), and *SIFUL2* (*pSIFUL2::fLUC*) as reporter. Numbers indicate technical replicates. Ctrl indicates no effector control. Letters represent post-hoc Tukey's HSD tests results with 95% confidence level.

Figure 3

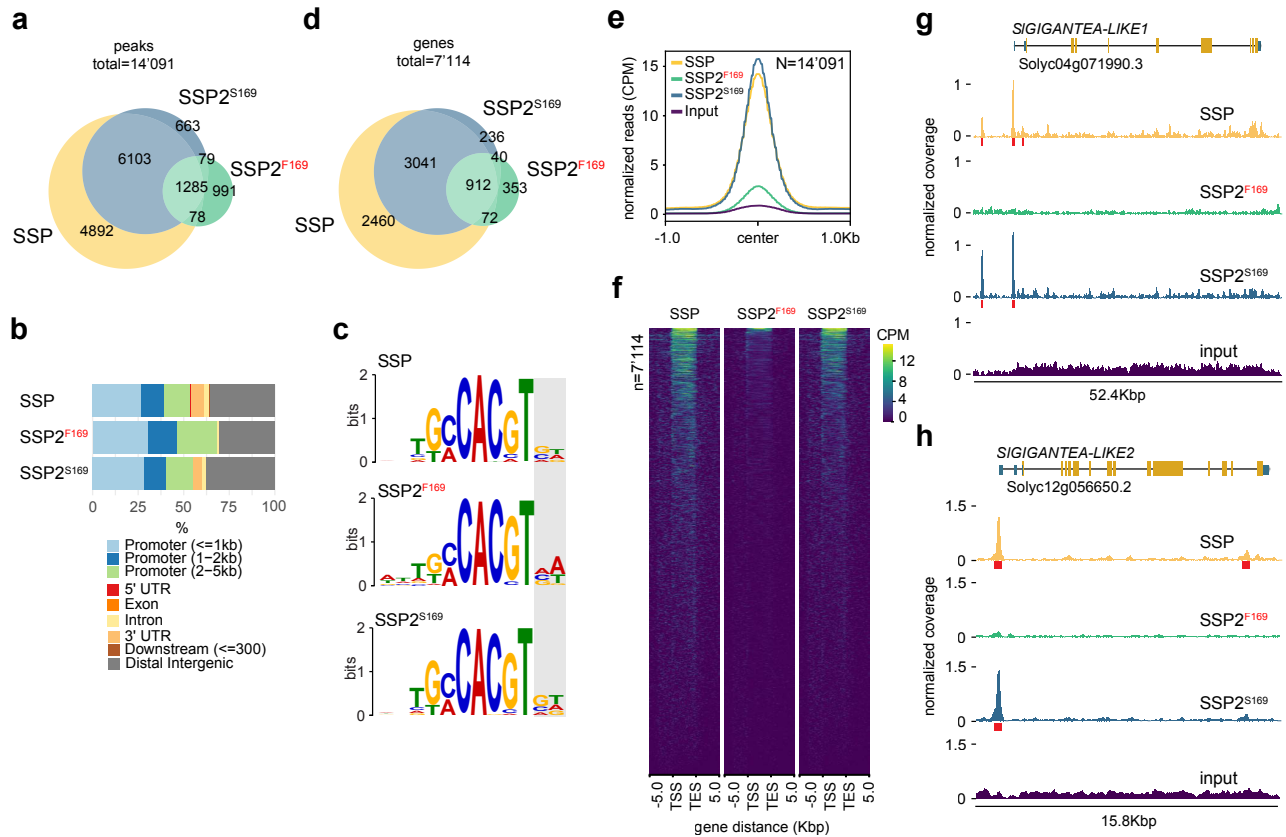


Figure 3: Domesticated SSP2^{F169} shows reduced binding at genome-wide target loci. **a**, Overlap of significant ($\log_2FC \geq 3$, $FDR \leq 0.01$) SSP, SSP2^{F169}, and SSP2^{S169} DAP-seq peaks ($n=14'091$). **b**, Distribution of significant SSP, SSP2^{F169}, and SSP2^{S169} DAP-seq peaks across gene features. **c**, Most-significant motifs identified by *de-novo* motif enrichment analysis of SSP, SSP2^{F169}, and SSP2^{S169} DAP-seq peak regions. Grey box delimits region with motif variation outside the core-motif. **d**, Overlap of genes with significant DAP-seq peaks ≤ 3 Kbp upstream and ≤ 2 Kbp downstream of the transcriptional start site ($n=7'114$). **e**, Profiles of normalized read coverage at significant SSP, SSP2^{F169}, and SSP2^{S169} peaks. **f**, Comparison of SSP, SSP2^{F169}, and SSP2^{S169} DAP-seq peaks relative to the transcriptional start (TSS) and end (TES) site of nearby genes ($n=7'114$). **g-h**, Browser view of SSP, SSP2^{F169}, and SSP2^{S169} DAP-seq peaks at *SIGIGANTEA-LIKE1* (**g**) and *SIGIGANTEA-LIKE2* (**h**). Normalized coverage (CPM) is shown in yellow, green and blue. Significant peak regions are indicated by red boxes.

Figure 4

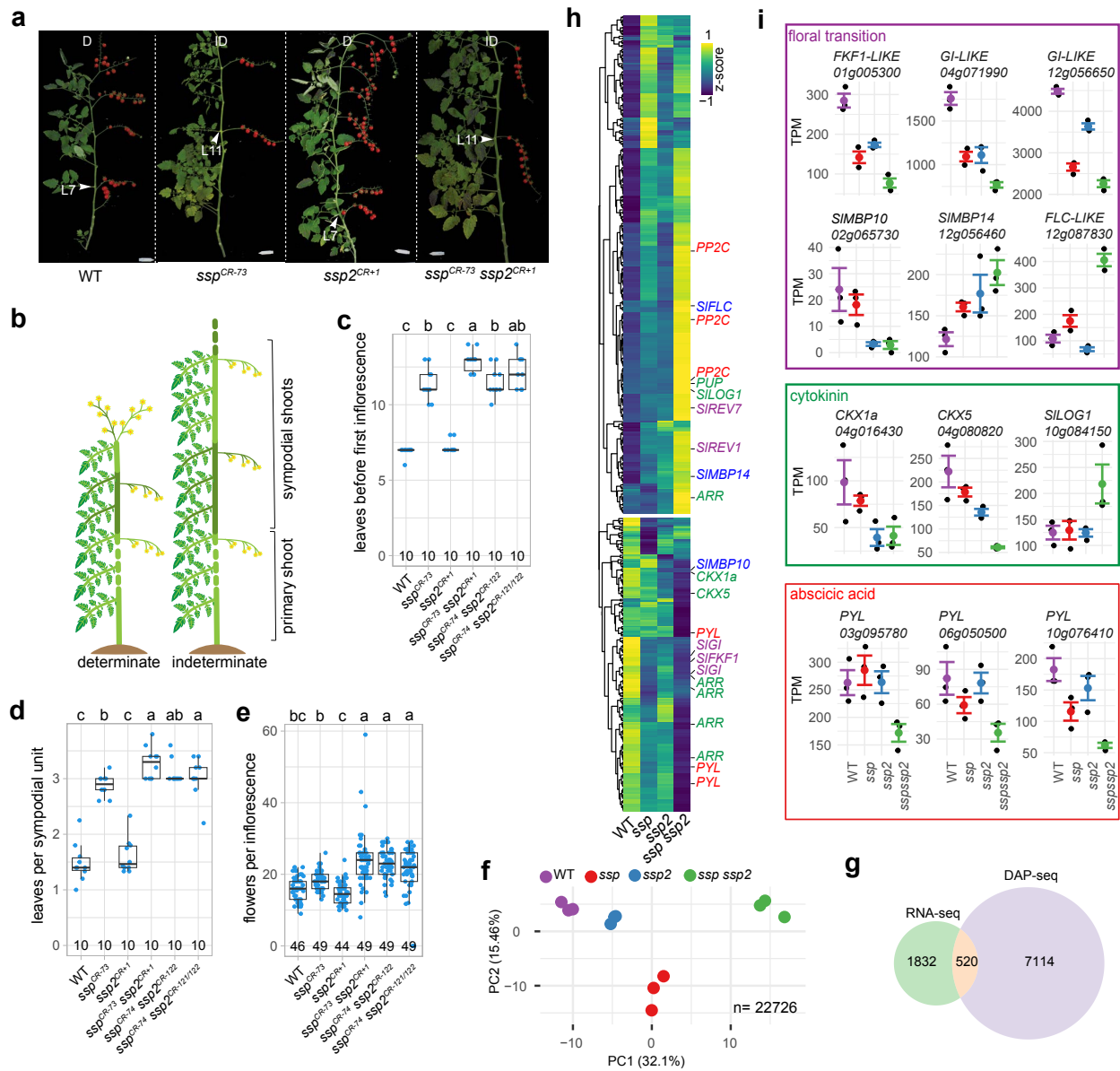


Figure 4: *SSP* and *SSP2* act partially redundant to regulate the transition to flowering. **a**, Representative images of wild-type S100, *ssp^{CR}* and *ssp2^{CR}* single mutants, and *ssp ssp2^{CR}* double mutants. L= leaf number, arrowheads mark the last leaf before flowering. Determinate (D) and indeterminate (ID) shoots are indicated. Scale bars represent 7.5 cm. **b**, Schematic depiction of tomato shoot architecture. Different shades of green delimit primary and sympodial shoots. **c-e**, Quantification of the floral transition (number of leaves before flowering) on the primary (c) and secondary (d) shoots, and the number of flowers per inflorescence (e) for genotypes shown in (a). The number of plants (c,d) and inflorescences (e) are indicated. Letters represent post-hoc Tukey's HSD tests results with 95% confidence level. **f**, Principal component analysis of 22,726 expressed genes in transition meristems of the WT, *ssp*, *ssp2*, and *ssp ssp2*, determined by RNA-seq. **g**, Overlap of genes differentially expressed ($\log_2FC \geq 0.58$, $FDR \leq 0.05$) in *ssp*, *ssp2*, and/or *ssp ssp2* with genes at SSP, SSP2^{F169}, and SSP2^{S169} DAP-seq peaks. **h**, Heatmap depicting expression of 520 putative SSP/SSP2 target genes. **i**, Normalized expression levels for selected putative direct targets. Genes are color coded based on the biological pathway.

Figure 5

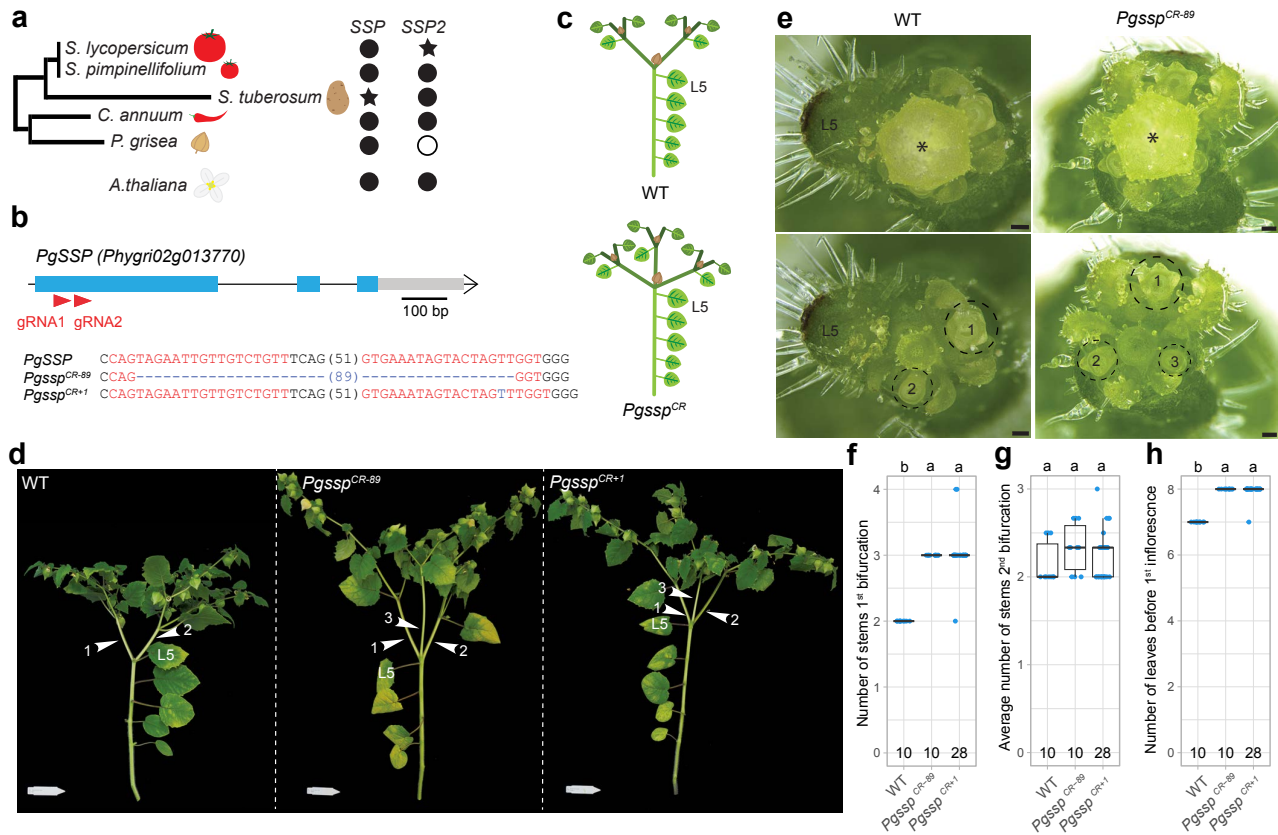


Figure 5: The genome of *Physalis grisea* encodes a single direct SSP ortholog that regulates meristem transitions. **a**, Scheme of the phylogenetic tree of tomato and closely related *Solanaceae* species. Filled circles, empty circles or star show presence, absence, or missense mutation, respectively, of SSP/SSP2 or FD/ FDP in these species. Full tree is displayed in Fig. S6. **b**, CRISPR-Cas9 targeting of *PgSSP* in *P. grisea*. Blue boxes, black lines, and grey boxes represent exonic, intronic, and untranslated regions, respectively. Single guide RNAs (sgRNAs) are indicated with red arrowheads. PAM and sgRNA sequences are indicated in black and red bold letters, respectively; deletions are indicated with blue dashes; sequence gap length is given in parenthesis. Insertions are indicated by blue letters. **c**, Model of the growth habit of *P. grisea* WT and *Pgssp^{CR}* plants. Different shades of green delimit primary, first sympodial, and second sympodial shoots. The color of leaves corresponds with the shoot of origin. Note that the last leaf of each shoot is displaced upwards during shoot development. **d**, Representative pictures illustrating the difference in number of sympodial shoots in WT and *Pgssp* mutant plants. Last leaf before the shoot bifurcation is indicated (L5). White arrowheads indicate individual sympodial shoots. Scale bar represents 7.5 cm. **e**, Representative stereoscope images of the shoot apex of WT and *Pgssp* mutant plants. Upper images show the apex with a terminal flower (*). Lower images show the same view with the flower removed. The sympodial meristems (SYMs) are delimited by a dashed line and numbered in developmental order. Scale bar represents 100 μ m. **f-h**, Quantification of the number of sympodial shoots at the first and second bifurcation, and flowering time (number of leaves before the first inflorescence). Number of plants is indicated at the bottom of the plots. Letters represent post-hoc Tukey's HSD tests results with 95% confidence level.

Figure 6

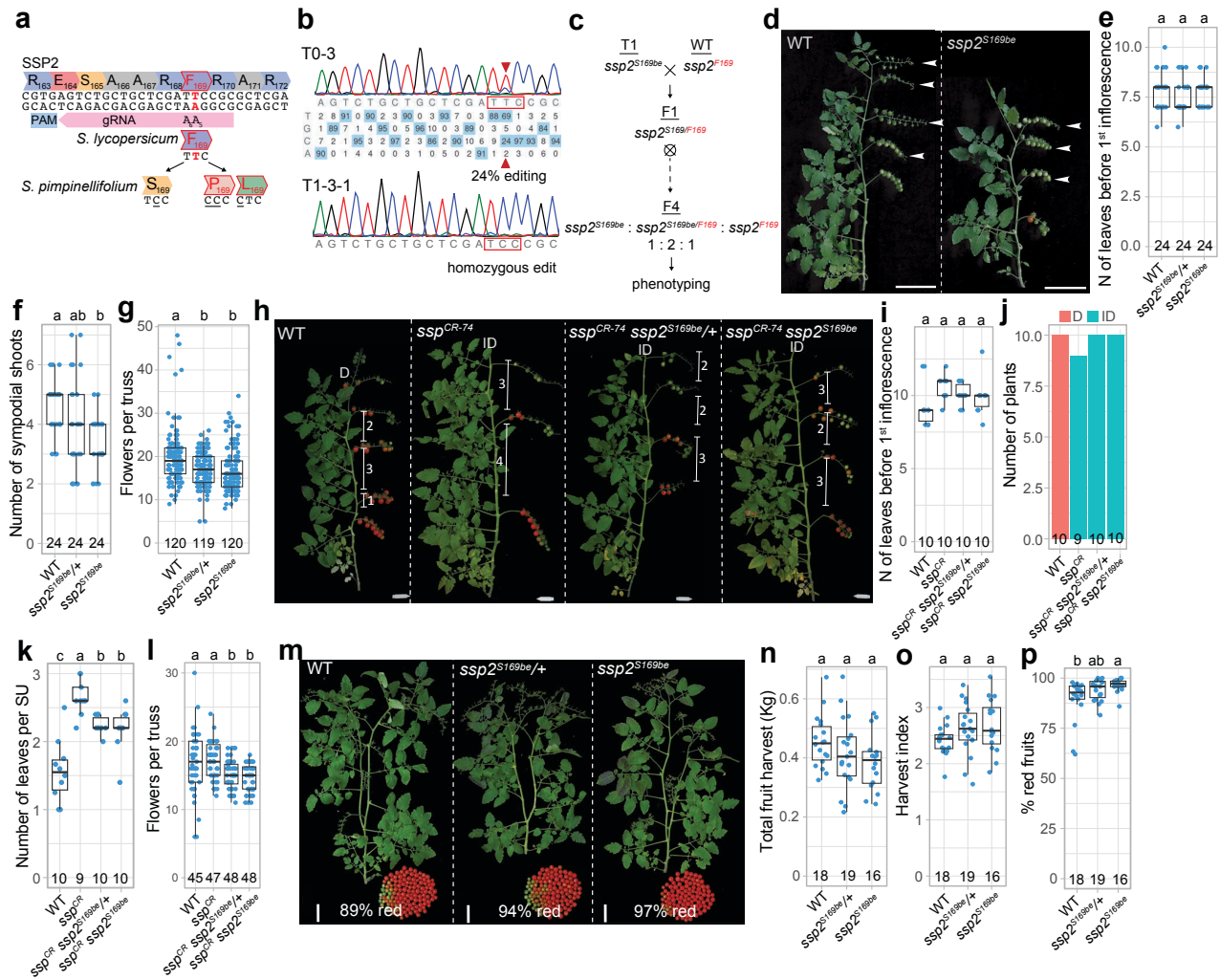


Figure 6: Repairing the deleterious *SSP2* mutation in domesticated tomato by base-editing leads to compact growth and earliness for yield. **a**, Base-editing strategy to correct the deleterious *SSP2* mutation in domesticated tomato using an adenosine base editor (ABE) and a PAM-less Cas9 variant. The target adenine in *SSP2* (A5) is at position 5 of the protospacer with a bystander adenine (A6) at position 6. Editing of the target codon (TTC) can lead to three different outcomes depending on which adenine is deaminated. Only editing the target nucleotide (A5) alone reverts the phenylalanine codon (TTC) back to the ancestral serine (TCC). **b**, Validation of editing in a chimeric first-generation (T0) transgenic and the corresponding T1 progeny by Sanger sequencing. The target nucleotide is indicated by a red arrowhead. **c**, Crossing scheme to generate the segregating *ssp2^{SI69be}* F4 population. **d**, Representative pictures showing the total number of sympodial units on WT and *ssp2^{SI69be}* plants. Terminal inflorescences of each sympodial unit are indicated by a white arrow. **e-g**, Quantification of flowering time (number of leaves before the first inflorescence), number of sympodial shoots, and number of flowers per truss of WT, *ssp2^{SI69be}/+* and *ssp2^{SI69be}* plants. **h**, Representative pictures showing the number of leaves per sympodial unit and determinacy of WT, *ssp^{CR}*, *ssp^{CR} ssp2^{SI69be}/+* and *ssp^{CR} ssp2^{SI69be}* plants. **i-l**, Quantification of flowering time (as in e), number of determinate plants, number of leaves per sympodial unit (SU), and number of flowers per truss of WT, *ssp^{CR}*, *ssp^{CR} ssp2^{SI69be}/+* and *ssp^{CR} ssp2^{SI69be}* plants. Determinate (D) and indeterminate (ID) shoots are indicated. **m**, Representative images showing the full harvest of individual WT, *ssp2^{SI69be}/+* and *ssp2^{SI69be}* plants. Percentage of red fruits is indicated. **n-p**, Quantification of total fruit yield (n), harvest index (total fruit yield / plant weight) (o), and percentage of red fruits. Number of plants are indicated in the plots for (e-g), (i-k) and (l-o). Letters on top of the plots represent post-hoc Tukey's HSD tests results with 95% confidence level. Scale bars represent 10 cm (d) and 7.5 cm in (h,m).

Figure S1

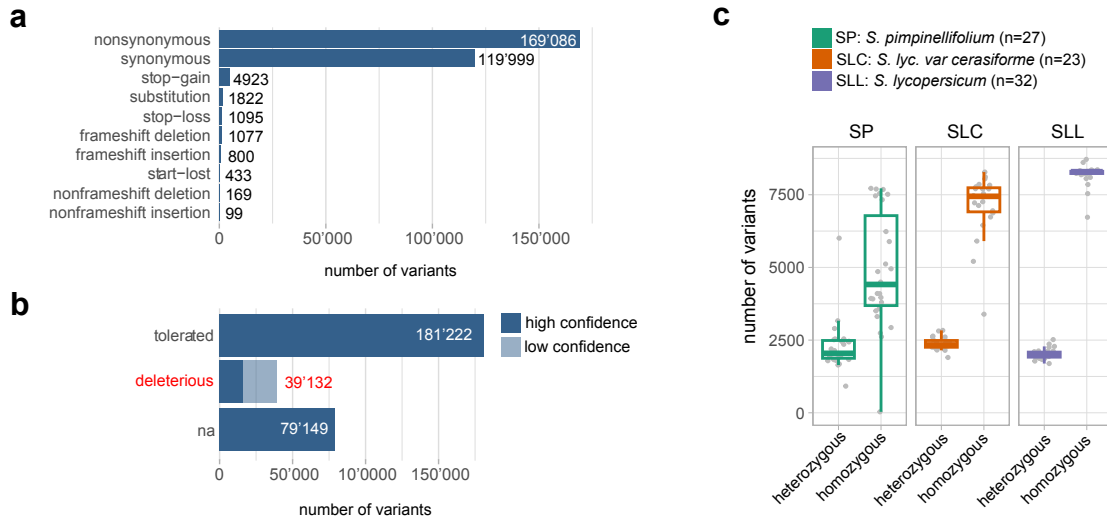


Figure S1: Prediction of deleterious variants in tomato. **a**, Number of coding sequence variants across a panel of 82 genomes. **b**, Number of non-synonymous variants predicted to be tolerated (sift-score ≥ 0.05), deleterious (sift-score < 0.05), or without prediction (na). Color code indicates confidence of SIFT prediction. **c**, Number of heterozygous and homozygous predicted deleterious mutations in wild (*S. pimpinellifolium*, n=27, in green), landrace (*S. lyc. var. cerasiforme*, n=23, in orange), and domesticated (*S. lycopersicum*, n=32, in purple) tomato genomes.

Figure S2

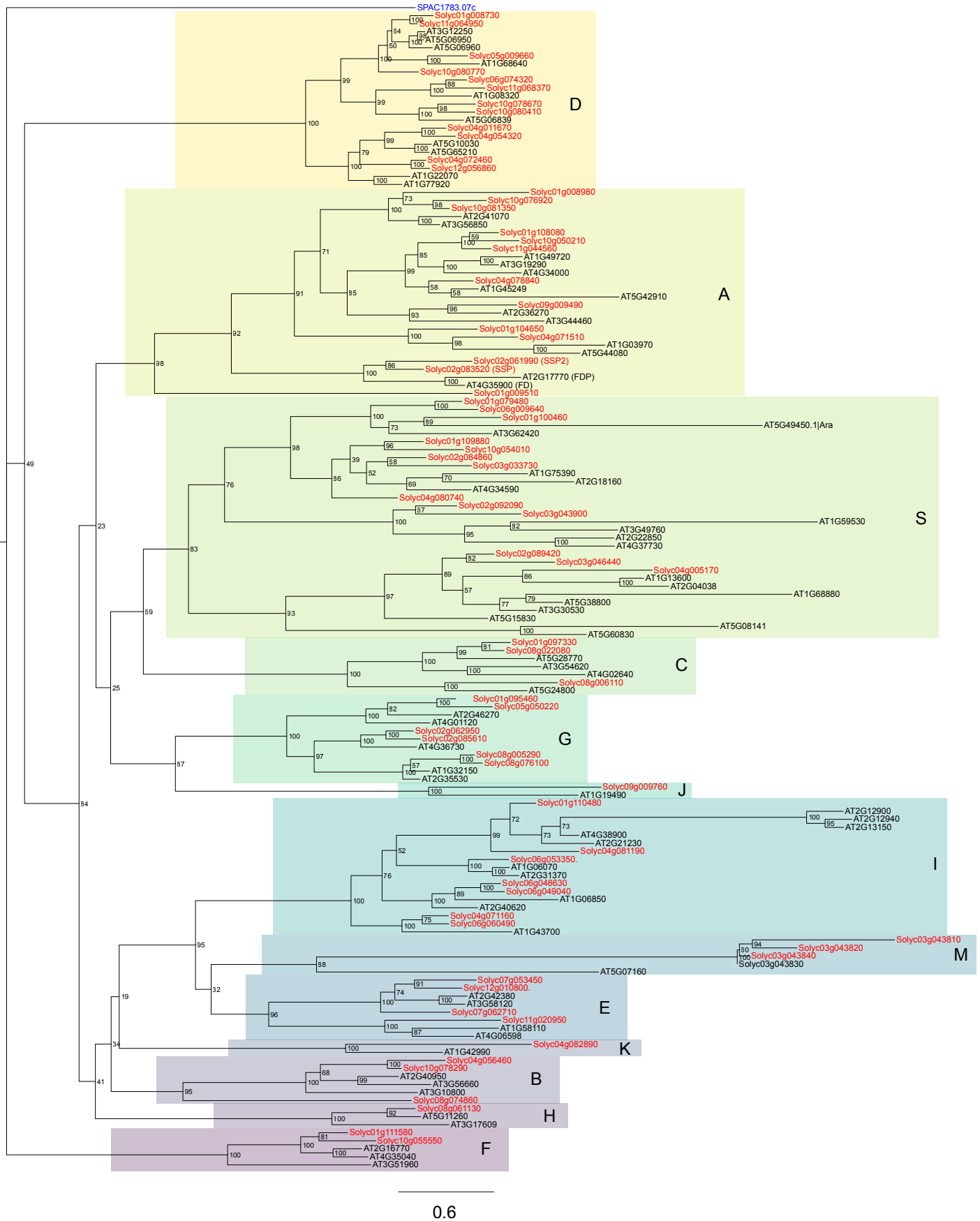


Figure S2: Phylogenetic analysis of the bZIP transcription factor family in Arabidopsis and tomato. Maximum-likelihood phylogenetic tree constructed with full-length bZIP protein sequences from Arabidopsis (n=74) and tomato (n=70). Arabidopsis and tomato proteins are indicated in black and red font, respectively. The yeast protein Pap1 was used as an outgroup (blue font). Proteins were classified into 13 groups (A-K, M, S) according to the Arabidopsis nomenclature ³⁷. Numbers represent bootstrap values from 1000 replicates, and scale bar indicates the average number of substitutions per site.

Figure S3

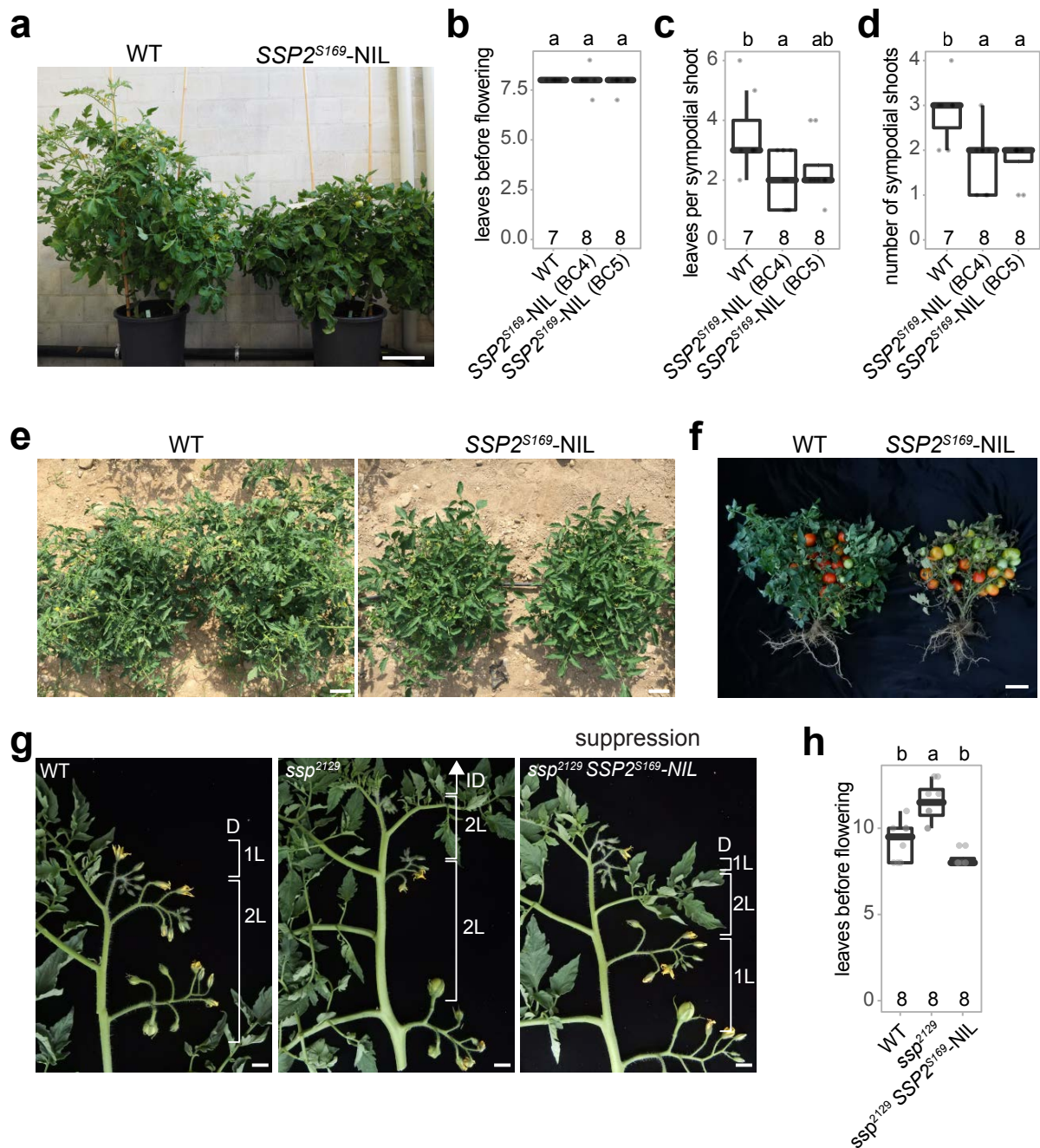


Figure S3: Introgression of ancestral $SSP2^{S169}$ into domesticated tomato suppresses late flowering and indeterminate growth of ssp mutants. **a**, Representative image of greenhouse-grown wild-type (WT) and $SSP2^{S169-NIL}$ individual in the determinate M82 background. **b-d**, Quantification of the floral transition (the number of leaves before flowering) on primary (b) and sympodial shoots (c), and the number of sympodial shoot units (d). **e, f**, Representative images of field-grown WT and $SSP2^{S169-NIL}$ plants at flowering (e) and fruiting (f) stage. **g**, Representative images of detached WT, ssp^{2129} and $ssp^{2129} SSP2^{S169-NIL}$ shoots (in the determinate M82 background). D, determinate; ID, indeterminate; L, leaves. **h**, Quantification of the floral transition on the primary shoot for genotypes shown in (e). Numbers at the bottom and letters at the top of the plots of (b) and (f) represent the number of replicate plants and post hoc Tukey's HSD test results with 95% confidence level, respectively. Scale bars indicate 10 cm (a, e, f) and 1 cm (g).

Figure S4

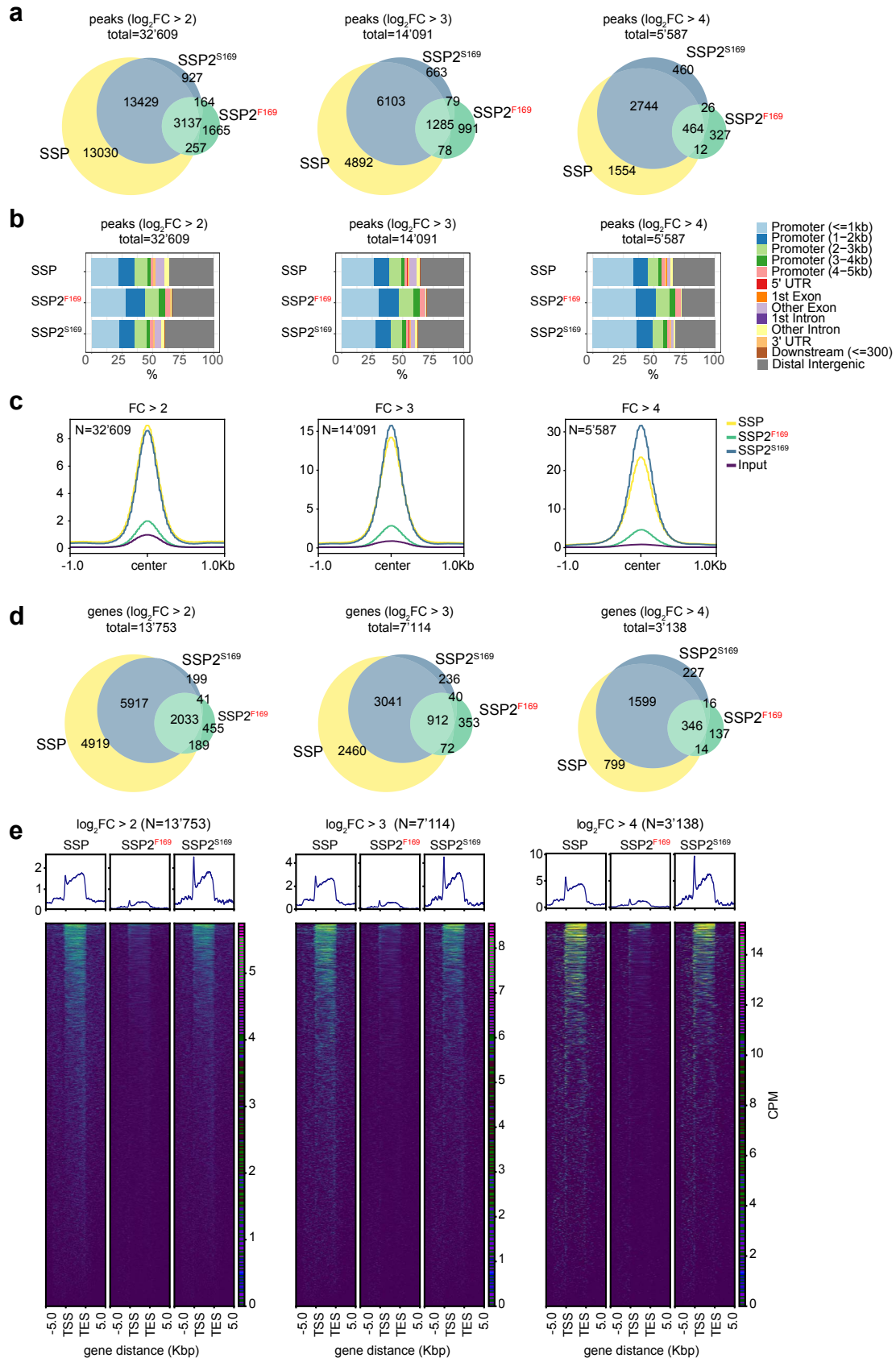


Figure S4: Identification of SSP, SSP2^{F169}, and SSP2^{S169} genome-wide binding sites by DAP-seq. **a**, Overlap of SSP, SSP2^{F169}, and SSP2^{S169} DAP-seq peaks at different significant thresholds ($\log_2FC \geq 2, 3, 4$). **b**, Distribution of SSP, SSP2^{F169}, and SSP2^{S169} DAP-seq peaks across gene features at different significant thresholds as in (a). **c**, Profiles of normalized read coverage at SSP, SSP2^{F169}, and SSP2^{S169} peaks at different significant thresholds as in (a). **d**, Overlap of genes with DAP-seq peaks ≤ 3 Kbp upstream and ≤ 2 Kbp downstream of the transcriptional start site, at different significant thresholds as in (a). **e**, Comparison of SSP, SSP2^{F169}, and SSP2^{S169} DAP-seq peaks relative to the transcriptional start (TSS) and end (TES) site of nearby genes, at different significant thresholds as in (a). Top and bottom panels show coverage profiles and heatmaps, respectively.

Figure S5

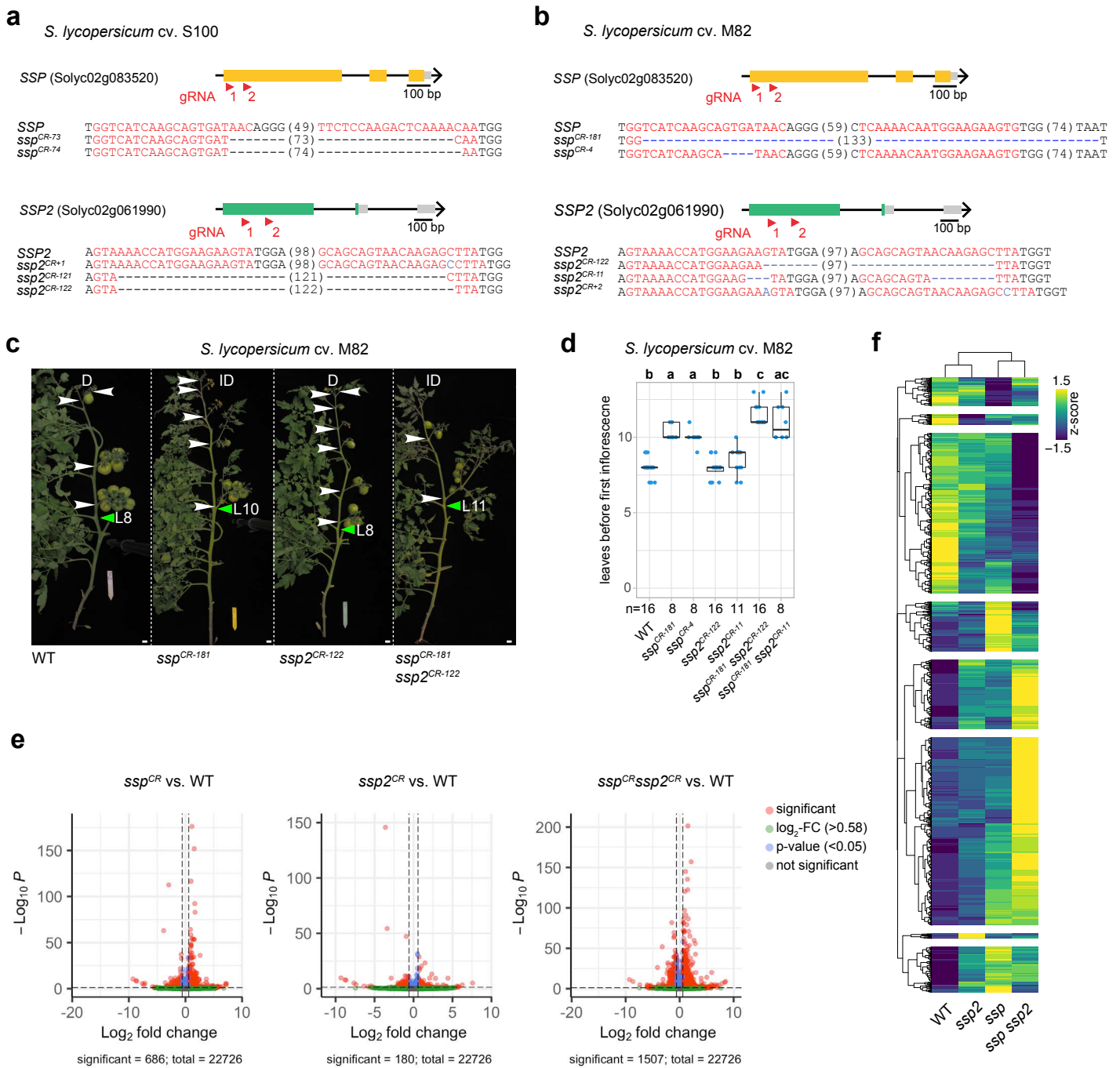


Figure S5: Targeting *SSP* and *SSP2* in two tomato cultivars by CRISPR-Cas9. **a,b** CRISPR-Cas9 targeting of *SSP* and *SSP2* in *S. lycopersicum* cv. S100 (a) and cv. M82 (b). Orange boxes, black lines, and grey boxes represent exonic, intronic, and untranslated regions, respectively. Single guide RNAs (sgRNAs) are indicated with red arrowheads. PAM and protospacer sequences are indicated in black and red bold letters, respectively; deletions are indicated with blue dashes; sequence gap length is given in parenthesis. **c**, Representative images WT S100, *ssp*^{CR} and *ssp2*^{CR} single mutants, and *ssp ssp2*^{CR} double mutants. L= leaf number, white arrowheads mark inflorescences. Determinate (D) and indeterminate (ID) shoots are indicated. Scale bars represents 1 cm. **d**, Quantification of the floral transition on the primary shoot for genotypes in (c). N, number of plants. Letters represent post hoc Tukey's HSD tests. **e**, Volcano plots showing differentially expressed genes (\log_2 FC > 0.58, FDR < 0.05) in *ssp*^{CR} and *ssp2*^{CR} single mutants, and *ssp ssp2*^{CR} double mutants compared to WT (cv. M82). **f**, Heatmap of z-scores showing expression pattern for 1'832 genes that are differentially expressed (\log_2 FC > 0.58, FDR < 0.05) in *ssp*^{CR}, *ssp2*^{CR} single mutants, and/or *ssp ssp2*^{CR} double mutants in M82.

Figure S6

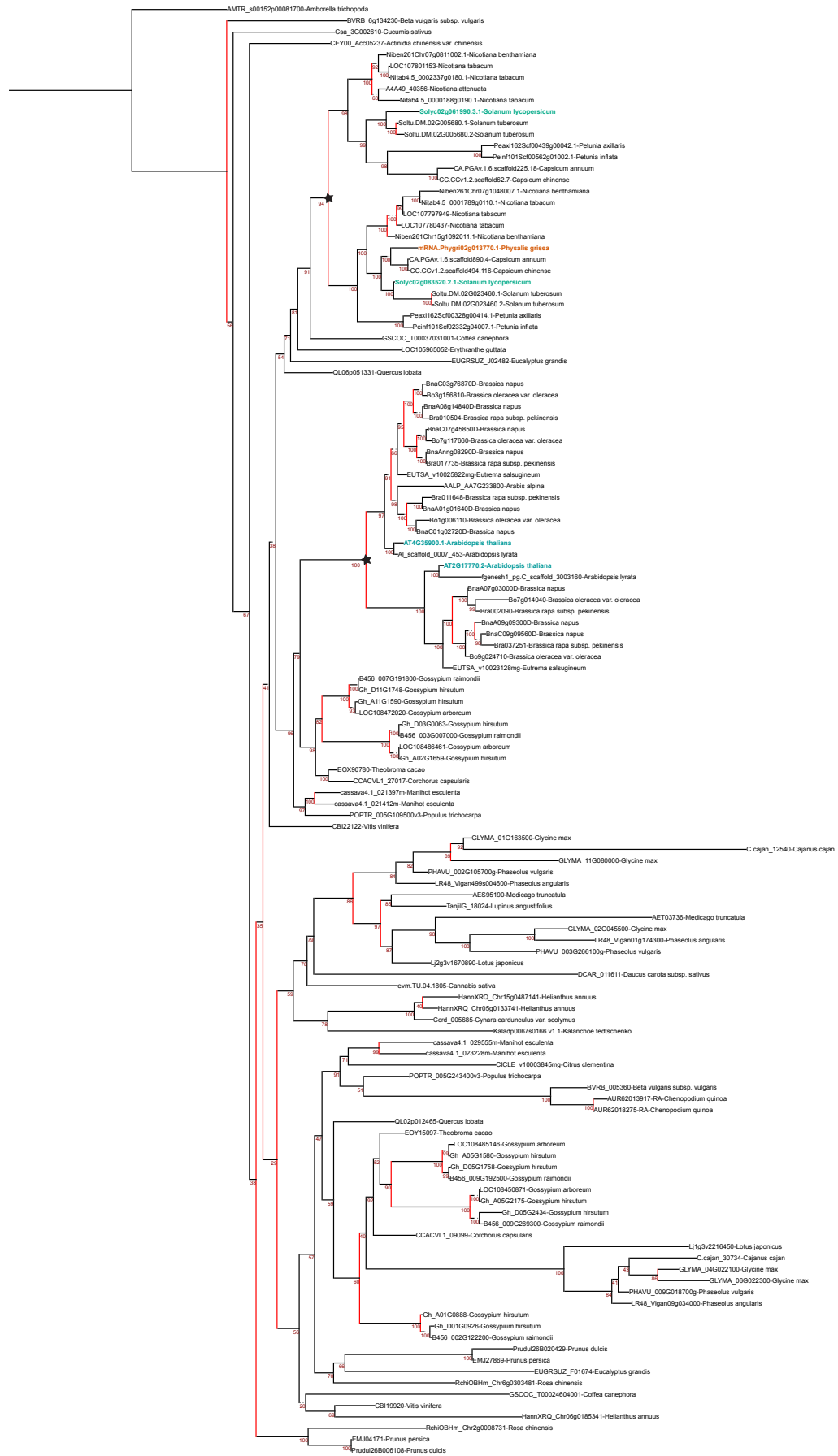


Figure S6: Phylogenetic analysis of SSP homologs in eudicots. Maximum-likelihood phylogenetic tree constructed with 128 full-length bZIP protein sequences from 51 eudicot species. Tomato, Arabidopsis, and Physalis proteins are highlighted in red, blue, and orange font, respectively. Red branches indicate duplication events, and the two separate duplication events in the *Solanaceae* and *Brassicaceae* are highlighted with stars. Numbers represent bootstrap values from 1000 replicates, and scale bar indicates the average number of substitutions per site.

Figure S7

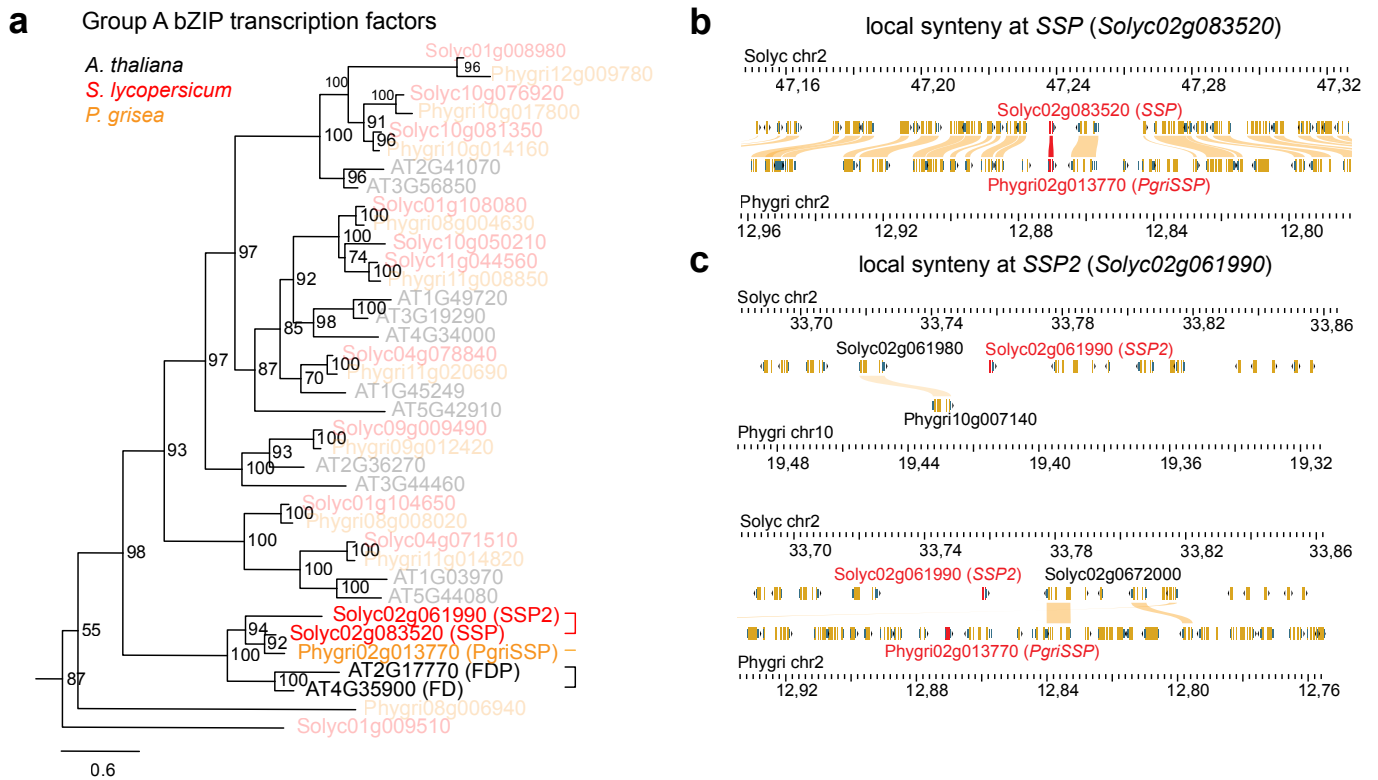


Figure S7: The ortholog of *SSP2* in *Physalis grisea* was lost during evolution. **a.** Maximum-likelihood phylogenetic tree of the group A bZIP transcription factor family of *A. thaliana*, *S. lycopersicum* and *P. grisea*. Numbers represent bootstrap values from 1000 replicates, and scale bar indicates the average number of substitutions per site. **b,c,** Browser view of synteny analysis of *SSP* (**b**) and *SSP2* (**c**) between tomato (cv. S100) and *P. grisea*. Yellow rectangles show annotated genes and yellow streaks link them with their syntenic counterpart. *SSP* and *SSP2* genes are indicated in red. Note the lack of a unique syntenic block for *SSP2* in *P. grisea* in (**c**).

Figure S8

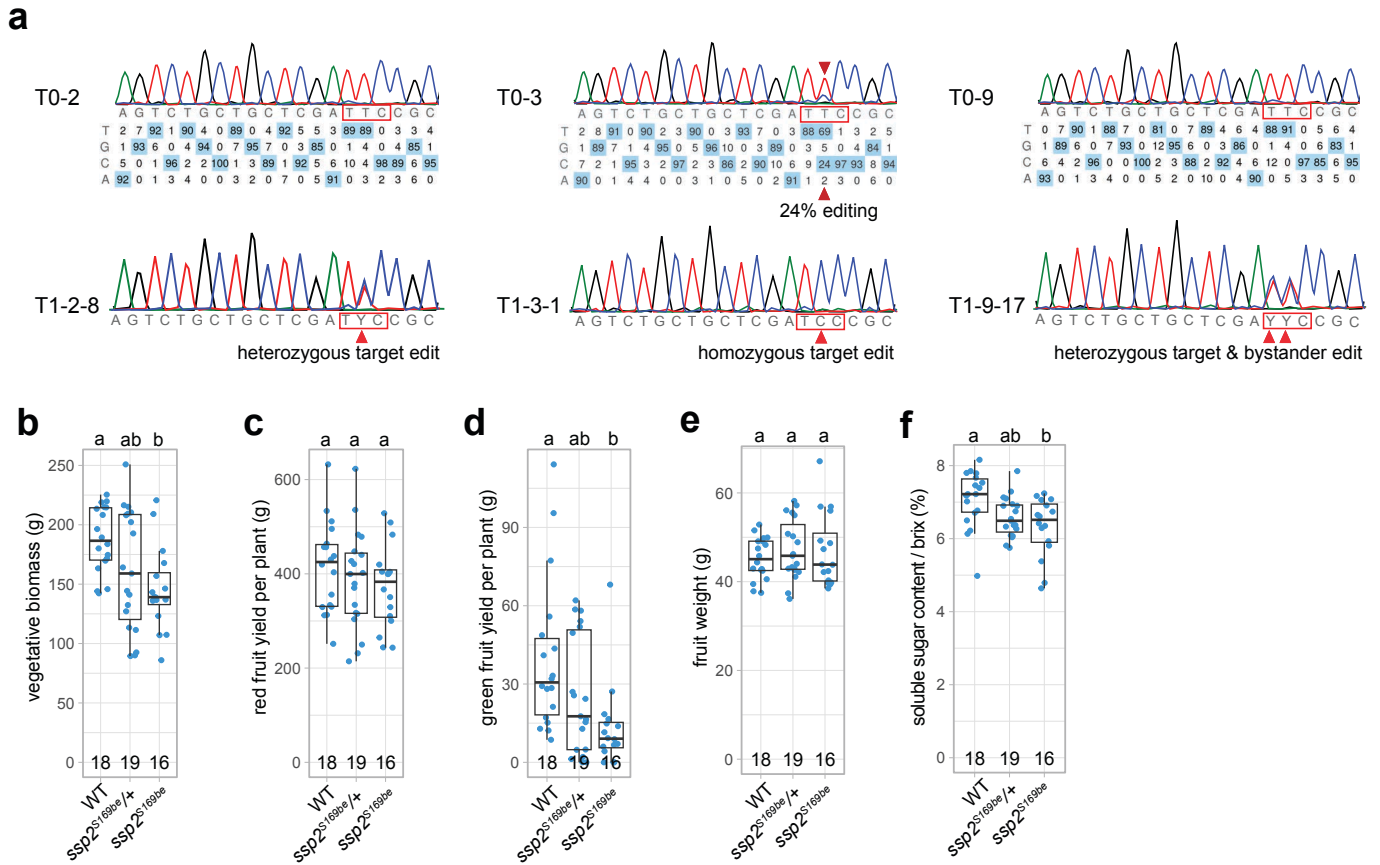


Figure S8: Base-editing of *SSP2* in domesticated tomato and its effect on different tomato yield components. **a**, CRISPR base-editing sequencing result of three T0 individuals (upper row) and their T1 progeny (lower row). Note that the target edit was detected in only one T0 individual (T0-3) but in three T1 families. One T1 individual (T1-9-17) was also edited at the bystander adenine. The edited nucleotides are indicated by a red arrowhead. **b-f**, Quantification of the vegetative biomass (b), total red and green fruit harvest (c,d), average fruit weight (e), and average soluble sugar content (brix) (f). The number of plants are indicated in the plots. Letters on top of the plots represent post-hoc Tukey's HSD tests results with 95% confidence level.